HHS Public Access

Author manuscript

J Immunol. Author manuscript; available in PMC 2016 May 15.

Published in final edited form as:

J Immunol. 2015 May 15; 194(10): 5022–5034. doi:10.4049/jimmunol.1402335.

General Approach for Tetramer Based Identification of Autoantigen Reactive B Cells: Characterization of La and snRNP Reactive B Cells in Autoimmune BXD2 Mice

Jennie A. Hamilton[*], **Jun Li**[*], **Qi Wu**[*], **PingAr Yang**[*], **Bao Luo**[*], **Hao Li**[*], **John E. Bradley**[*], **Justin J. Taylor**[†], **Troy D. Randall**[*], **John D. Mountz**[*,‡], and **Hui-Chen Hsu**[*]

[*]Division of Clinical Immunology and Rheumatology, Department of Medicine, Birmingham, AL, 35294

[†]Vaccine and Infectious Disease Division, Fred Hutchinson Cancer Research Center, Seattle, WA, 98109

[‡]Department of Medicine, Birmingham VA Medical Center, Birmingham, AL, 35233

Abstract

Autoreactive B cells are associated with the development of several autoimmune diseases, including systemic lupus erythematosus (SLE) and rheumatoid arthritis (RA). The low frequency of these cells represents a major barrier to their analysis. Antigen-tetramers prepared from linear epitopes represent a promising strategy for the identification of small subsets of antigen-reactive immune cells. This is challenging given the requirement for identification and validation of linear epitopes and the complexity of autoantibody responses, including the broad spectrum of autoantibody specificities and the contribution of isotype to pathogenicity. We therefore tested a two-tiered peptide microarray approach, coupled with epitope mapping of known autoantigens, to identify and characterize autoepitopes using the BXD2 autoimmune mouse model. Microarray results were verified through comparison with established age-associated profiles of autoantigen specificities and autoantibody class switching in BXD2 and control (B6) mice and high-throughput ELISA and ELISPOT analyses of synthetic peptides. Tetramers were prepared from two linear peptides derived from two ribonucleic acid binding proteins (RBP): lupus La and 70 kDa U1 small nuclear ribonucleoprotein (snRNP). Flow cyotmetric analysis of tetramer-reactive B-cell subsets revealed a significantly higher frequency and greater numbers of RBP-reactive marginal zone precursor (MZ-P), transitional T3 and PDL-2^{+}CD80^{+} memory B cells, with significantly elevated CD69 and CD86 observed in RBP^{+} MZ-P B cells in the spleens of BXD2 compared to B6 mice, suggesting a regulatory defect. This study establishes a feasible strategy for the characterization of autoantigen-specific B-cell subsets in different models of autoimmunity and, potentially, humans.

Corresponding author: Hui-Chen Hsu, Ph.D, Shelby 311, 1825 University Blvd, Birmingham, AL 35294, USA, Phone: 205-934-8909, Fax: 205-996-6788, Rhue078@uab.edu.

Introduction

Autoantibody production by autoreactive B cells is characteristic of many autoimmune diseases, including SLE and RA (1, 2). Studies using mouse models indicate that certain autoantibodies can drive the development of these diseases (3–5). In humans, the close association of some autoantibodies with disease activity and progression together with the therapeutic effects of B cell depletion suggests their role in clinical disease (6, 7). Although disrupted regulation of autoreactive B cells is considered central to the development of autoimmunity, the relative contributions of different subsets of B cells (8, 9) remains unclear. Progress in this area is challenged by the low frequency of the autoreactive B cells and their diversity, which encompasses the broad spectrum of autoantigens recognized, the isotype of the antibodies produced and the subtle phenotypic distinctions that differentiate B cell subsets. To date, the most commonly used approach to analysis of autoantigen-specific B cell subsets in autoimmunity has been the creation of transgenic mice in which the cells can be expanded clonally through experimental manipulation (10).

Labeled monomeric and tetrameric antigen conjugates can be used to brightly label cells on the basis of their ligand specificity (11, 12). This approach has been applied successfully to the identification and isolation of specific types of cells that occur at low frequency (13, 14). It is, however, technically difficult to construct a labeled autoantigen tetramer using most full-length antigens, as the process requires ligation of the antigen-coding material into an expression vector with a biotinylated site and, subsequently, stringent purification of the antigen. One approach to overcome this issue is the use of small, linear-peptide autoepitopes. In 2003, Newman, *et al.* described a system in which a DNA mimetope peptide could be conjugated to phycoerythrin (PE)-labeled streptavidin (SA) and used to detect B cells reactive to this DNA mimetope in immunized BALB/c mice (15) and later in humans with SLE (16). This tetramer strategy has since been adapted for the isolation of B cells specific for various epitopes on citrullinated fibrinogen (17), HLA (18) HIV gp41 (19, 20), and tetanus toxoid C fragment (11). Recently, Taylor *et al*. used a novel detection and tetramer enrichment strategy to assess polyclonal self-antigen-specific B cells by rigorously analyzing regulation of ovalbumin (OVA) and glucose-6-phosphate isomerase (GPI) Ag-specific B cells in OVA expressing and wild-type mice (21).

Potentially, the epitope-tetramer approach represents a powerful tool for analysis of B-cell reactivity in autoimmunity, especially if it could be applied to analysis of B cells that are reactive with the predominant autoantigens that have been identified in SLE and RA. Full realization of this potential depends, however, on a feasible strategy for the identification and characterization of linear autoepitopes and the demonstration that these linear autoepitopes represent authentic, clinically relevant antigens. Since the first description of the development of large-scale autoAg arrays for autoAb determination in patient sera (22), advances in peptide microarray chip technologies have led to the development of comprehensive Ag-arrays (23, 24). We reasoned that these arrays, which contain thousands of known B-cell epitopes and their modified variants, can be used to identify authentic linear autoepitopes that are potential candidates for the generation of autoAg-tetramer panels.

To test this strategy, we used a step-wise approach to enable identification of lupus La and snRNP autoepitopes reactive with B cells from the BXD2 mouse model of systemic autoimmunity. The emergence of the autoantibody repertoire and, importantly, its age-associated transition to the expression of pathogenic autoantibodies is well characterized in these mice (4, 25, 26). Utilization of these tetramers for FACS sorting of B cells from the spleens of BXD2 and B6 mice confirmed an expanded frequency and number of $La_{13–27}$ and $snRNP_{357–373}$ epitope-reactive, activated ($CD69^+$ and $CD86^+$) MZ-P B cells in BXD2 mice as compared to age-matched B6 mice and further revealed an expanded frequency and higher number of $La_{13–27}$ and $snRNP_{357–373}$ reactive transitional T3 and memory B cells. Thus, the present work validates the utilization of linear autoepitopes for analysis of the autoantibody repertoire and establishes a systematic, experimental approach to autoepitope identification and Ag tetramer-based B-cell isolation. This approach is readily adaptable to analysis of other autoimmune models and, potentially, analysis of patient-derived samples.

Materials and Methods

Mice

Female C57BL/6 (B6) and BXD2/TyJ recombinant inbred mice were obtained from The Jackson Laboratory. All mice were housed in the University of Alabama at Birmingham Mouse Facility under specific pathogen-free conditions in a room equipped with an air-filtering system. The cages, bedding, water, and food were sterilized. All mouse procedures were approved by the University of Alabama at Birmingham Institutional Animal Care and Use Committee. Sera were obtained from B6 and BXD2 mice at the specified ages by retro-orbital eye bleeding. After separation from blood, sera were stored at −80°C.

Peptide Microarray

Autoantibody profiles for linear peptides were determined using PEPperCHIP® technology (PEPperPRINT GmbH, Heidelberg, Germany). For the PEPperCHIP® Autoimmune Epitope Microarray, 2,733 autoimmune disease-associated linear B-cell epitopes were selected unbiasedly using all linear epitopes that have been curated for humans or mouse models of autoimmune diseases from the Immune Epitope Database (27) (http://www.iedb.org/) including 192 citrullinated peptides. Longer peptides with more than 15 aa were translated into overlapping 15 aa peptides with a peptide-peptide overlap of 14 aa, resulting in 3,830 total peptides on the chip. Peptides shorter than 3 amino acids and peptides including non-citrulline side-chain modifications were not included on the chip. Peptides were all printed in duplicate spots and framed by a fusion tag (Flag) peptide (DYKDDDDKGG, 186 spots) and influenza virus hemagglutinin (HA) epitope tag peptide (YPYDVPDYAG, 186 spots) as controls. Controls were detected by monoclonal anti-FLAG(M2)-LL-DyLight800 and monoclonal anti-HA (12CA5)-LL-DyLight680 (1:1000) (Rockland Immunochemicals, Inc., Gilbertsville, PA).

The microarray was initially incubated with the secondary goat anti-mouse IgG (H+L) DyLight680 antibody at a dilution of 1:5000 for 60 min at room temperature to analyze background interactions with the autoimmune epitopes, ensuring that there were no background interactions due to non-specific binding of the secondary antibody to the

peptides. Serum from six 8–10 month old BXD2 mice was pooled. Before serum incubation with chip, peptide arrays were first incubated for 60 min in Blocking Buffer for Near Infra Red Fluorescent Western blotting (Rockland Immunochemicals, Inc., Gilbertsville, PA). The microarray was washed twice in PBS, pH 7.4 with 0.05% Tween 20 (PBS-T), and incubated for an additional 30 min in washing buffer. The array was then incubated overnight at 4°C with mouse sera diluted 1:1000 for anti-mouse IgG (H+L) analysis or 1:200 for gamma-chain-specific and 1:1000 for μ-chain-specific analysis in PBS-T (secondary anti-mouse Ig Abs from Rockland Immunochemicals, Inc., Gilbertsville, PA). After multiple washes in washing buffer, the microarrays were incubated for 30 min with the secondary antibody in PBS-T at room temperature. After two additional washes in washing buffer, the microarrays were rinsed with ultrapure water and dried in a stream of air.

Green/red fluorescence intensities were acquired on an LI-COR Odyssey Imager (Lincoln, NE) at scanning intensities of 7/7 in both channels (700 nm/800 nm), 0.8 – 1.0 mm offset, at a spatial resolution of 21 μm. Staining of the Flag and HA control peptides that frame the arrays gave rise to high and homogeneous spot intensities with a coefficient of variation of <2%. PepSlide® Analyzer software was used to analyze the data. This program breaks down the fluorescence intensities of each spot into raw, foreground, and background signals, and calculates the standard deviation of the foreground median intensities. Epitopes resulting in a binding intensity greater than five standard deviations from mean chip intensity were considered as positive.

A custom epitope microarray with 80 epitopes selected based upon the first array analysis was then prepared (PEPperCHIP® GmbH). Analysis of serum from individual B6 and BXD2 mice of different ages was carried out in the same fashion as the first microarray (serum dilution 1:200 for IgG analysis, 1:1000 for IgM analysis). IgG and IgM reactivity was detected by goat anti-mouse IgG conjugated DyLight800 and goat anti-mouse IgM (μ chain) conjugated to DyLight680 at 1:1000 and 1:5000 dilutions respectively (both Rockland Immunochemicals, Inc., Gilbertsville, PA). For these analyses, epitopes resulting in a binding intensity of five-fold or greater compared to B6 control mice were considered positive. Lastly, pooled sera from B6 and BXD2 mice were used to probe the 2.0v Autoimmune Epitope Microarray, containing 4,389 peptides from the IEDB (PEPperCHIP® GmbH).

Tetramer production

Lupus $La_{13–27}$ LEAKICHQIEYYFGD) and $SnRNP_{357–373}$ SHRSERERRRDRDRDRD) were produced and biotinylated at the N-terminus by Sigma-Aldrich and supplied as a lyophilized powder. Each peptide was suspended in DMSO to a stock concentration of 10 mM and diluted to 1 mM in pure dH2O. Suspended peptides were aliquoted and stored at −80°C. Tetramers were generated by adding biotinylated peptide step-wise in 1/10 volumes to 6.7 μM streptavidin-R-phycoerythrin (SA-PE, ProZyme) at a molar ratio of 30:1 and allowed to incubate 60 min at room temperature or overnight at 4°C. Tetramers were purified on a Sephacryl S-300 FPLC size exclusion column. The tetramer fraction was concentrated using a 100-kDa molecular weight cutoff Amicon Ultra filter (Millipore). The concentration of tetramer was calculated by comparison with a standard curve of PE

absorbance at 540 nM, which was measured using an Emax Precision Microplate Reader (Molecular Devices, Sunnyvale, CA).

The nonspecific tetramer control was prepared by conjugating the core fluorochrome SA-PE to AF647 (Molecular Probes) according to the manufacturer's protocol for 60 min at room temperature. The free AF647 was removed by centrifugation in a 100-kD molecular weight cut off Amicon Ultra filter (Millipore). The SA-PE*AF647 complex concentration was calculated by measuring the absorbance of PE at 540 nm. The SA-PE*AF647 complex was then incubated with 10-fold molar excess of free biotin for 30 min at room temperature.

Tetramer enrichment

Spleens were harvested from individual mice and single-cells suspensions prepared in RPMI supplemented by 5% fetal bovine serum (FBS). Cell suspensions were prepared by gentle teasing apart of tissue with the plunger of a 3 mL syringe. Cells were passed through a cell strainer to eliminate clumps and debris and washed with RPMI. Red blood cells were lysed from the resuspended pellet with 3–5 mL ACK lysing buffer and washed twice in RPMI. Lymphocytes were resuspended to 200 μl in anti-CD16/32 Fc block (2.4G2; BioLegend) in 2% rat serum. Next, PE*AF647-conjugated nonspecific tetramer was added at a concentration of 20–30 nM and incubated at 4°C for 5–10 minutes. PE-conjugated peptide tetramer was added at a concentration of 10–20 nM and incubated on ice for 30 min, followed by one wash in 15 ml cold fresh sorter buffer (PBS, 2 mM EDTA, 2% FBS). Tetramer-stained cells were then resuspended to a volume of 80 μl of sorter buffer per 10^7 cells, mixed with 5–10 μl anti-PE–conjugated magnetic microbeads (Miltenyi Biotec) per 10^7 cells and incubated on ice for 30 min, followed by one wash with 10 ml sorter buffer. In experiments where single-cell suspensions were divided into 1/2 and 1/4 mouse equivalents before tetramer labeling/enrichment, the volumes were scaled down appropriately. The cells were then resuspended in 3 ml of cold sorter buffer and passed over a magnetized LS column (Miltenyi Biotec). Bound cells were eluted according to manufacturer's instructions. Free peptide blocking experiments were performed on unenriched samples. Free peptide (300 μM) was allowed to incubate with cells 30 minutes prior to tetramer staining.

Flow cytometry analysis

Cell pellets from the enriched and column flow-through fractions were re-suspended in FACS buffer (PBS + 5% FBS) and incubated with surface antibodies for 30 min on ice. Surface antibodies included Pacific Blue–anti-CD19 (6D5; BioLegend) or Brilliant Violet 650-anti-CD19 (6D5; BioLegend), Brilliant Violet 605-anti-CD86 (GL-1; BioLegend), Brilliant Violet 510-anti-CD69 (H1.2F3; BioLegend), FITC-anti-CD21/35 (7E9; BioLegend), PE-Cy7-anti-F4/80 (BM8 BioLegend), PE-Cy7-anti-Thy1.2 (30-H12; BioLegend) and FITC anti-CD93 (AA4.1, Biolegend). Dead cells were excluded from analysis wtih APC-eFluor® 780 Organic Viability Dye (eBioscience). After cell surface staining, cells were washed twice with 3 mL FACS buffer and fixed in 1% paraformaldehyde/FACS solution for cell surface marker analysis. Cells (300,000–1 X 10^6 / sample) were analyzed by flow cytometry. FACS data were acquired with an LSRII FACS analyzer (BD Biosciences) and analyzed with FlowJo software (Tree Star Ashland, OR). All flow cytometry analysis was carried out using a combination use of forward light scatter and

side scatter height, area, and width parameters to exclude aggregated cells. B cell population gating strategy was carried out based on the method described by Allman and Pillai (28).

ELISA

The levels of autoantibodies specific for selected linear peptides in the sera of B6 and BXD2 mice were determined by ELISA using a NeutrAvidin High Binding Capacity-coated 96-well plate (Thermo Scientific Pierce). Briefly, biotinylated peptides were conjugated to the plate overnight at 4°C at a concentration of 30 μM (all peptides were purchased from Sigma Aldrich). ELISAs were developed with either an HRP-labeled goat anti-mouse IgG or a goat anti-mouse IgM Ab (Southern Biotechnology Associates) and tetramethylbenzidine substrate (Sigma-Aldrich). $OD_{450–650}$ was measured on an Emax Microplate reader.

ELISPOT quantification of autoantibody-producing B cells

NeutrAvidin High Binding Capacity coated plates (96 well) (Thermo Scientific Pierce) were coated overnight with 50 μM of peptide at 4°C, washed, and then blocked with complete medium. Single cell suspensions of spleens isolated from B6 or BXD2 mice were prepared as described above followed by erythrocyte removal by ACK lysis. Cells were washed twice and adjusted to a final volume of 200 μl containing 1×10^5 cells/well in the presence or absence of phorbol myristate acetate (PMA; 50 ng/ml; Sigma-Aldrich) and ionomycin (750 ng/ml; Sigma-Aldrich) which stimulates the calcineurin pathway and B cell affinity maturation (29). After incubation for 24 h, plates were washed six times with PBS/0.05% Tween 20 and then incubated for 4 h with1 μg/ml HRP-conjugated goat anti-mouse IgM mAb (Southern Biotechnology Associates) or HRP-conjugated goat anti-mouse IgG (Southern Biotechnology Associates) in PBS/5% BSA. Plates were washed six times with PBS/0.05% Tween 20, before spots were developed using 3-amino-9-ethylcarbazole. Plates were read using a CTL automatic ELISPOT reader and analyzed using Immunospot 3.1 software (CTL). All experiments were repeated in duplicate.

B cell stimulation

For some experiments, different populations of $tetramer^+$, non-specific and $tetramer^{neg}$ B cells were sorted on a FACSAria and cultured in the presence of LPS (Sigma Aldrich, 20 μg/mL) and IL-4 (100 units/mL) for four days. The supernatant was collected and used immediately or stored at −80°C until analysis of reactivity for the secreted IgG autoantibodies.

Full Length Protein and Western Blot Analysis

Full length human recombinant La was purchased from ProSpec-Tany Technogene Ltd. La protein was uniformly uploaded, electrophoresed on 12% SDS polyacrylamide gels and transferred onto polyvinylidene difluoride membranes. The membranes were incubated with supernatant from cultured cells overnight at 4 °C. As a positive control, anti-La antibody (Cell Signaling Technology) was used at a dilution of 1:1000 to confirm the identity of the La protein on the blot. Anti-mouse or anti-rabbit HRP-conjugated Abs (Life Technologies) were used at a 1:250 dilution. HRP Abs were detected using a chemiluminescent substrate (Pierce).

Statistical Analyses

All results were shown as mean ± standard error of the mean (SEM). A two-tail *t* test was used when two groups were compared for statistical differences. *P* values less than 0.05 were considered significant. For microarray antigen distribution analyses, Chi squared analysis was performed, and a p-value less than 0.05 was considered significant.

Accession numbers

Microarray data were deposited in GEO, with master accession number GSE65290 (http://www.ncbi.nlm.nih.gov/geo/query/acc.cgi?acc=GSE65290). GEO accession numbers for data shown in Figure 1 and Figure 2 are GSE65276 (http://www.ncbi.nlm.nih.gov/geo/query/acc.cgi?acc=GSE65276) and GSE65234 (http://www.ncbi.nlm.nih.gov/geo/query/acc.cgi?acc=GSE65234), respectively. GEO accession numbers for data shown in Supplementary Figure 1 are GSE65277 and GSE65278 (http://www.ncbi.nlm.nih.gov/geo/query/acc.cgi?acc=GSE65277 and http://www.ncbi.nlm.nih.gov/geo/query/acc.cgi?acc=GSE65278, respectively).

Results

Identification of autoAg-derived peptides recognized by antibodies from BXD2 mice

To test whether autoimmunity epitope microarray could be used to identify linear autoepitopes in the sera of autoimmune BXD2 mice, we used pooled sera from six BXD2 mice that developed spontaneous lupus-like features (8–10-month old). The microarray consists of 2,733 experimentally characterized autoimmune epitopes and 192 citrullinated variants. All of these epitopes have been associated with autoimmune disease and are cataloged in the Immune Epitope Database (IEDB) (30). For our analyses, chip epitopes derived from non-mammalian species were not included. The BXD2 serum peptide-reactivity profile was detected by goat-anti-mouse IgG, revealing that the majority (79%) of BXD2 reactive autoepitopes derive from three main groups: nuclear proteins, endoplasmic reticulum (ER) or mitochondrial enzymatic proteins, and matrix proteins (Fig. 1*A*). There was a significantly increased prevalence of reactivities to peptides deriving from nuclear Ags and ER/mitochondrial enzymatic proteins (Fig. 1*A*) and within the nuclear Ags, an increase in peptides deriving from ribonucleoprotein (RNP) Ags (Fig. 1*B*). These results are consistent with our previous MALDI-TOF-MS analysis of BXD2 autoantibody-precipitated autoantigens resolved by 2-dimensional electrophoresis, in which the major autoAgs targeted by serum from 8–10 month old BXD2 mice were identified as nuclear proteins (snRNP, Ro, histone), heat-shock proteins (GRP78 or “BiP”), enzymes (enolase, aldolase), and structural proteins (keratin, actin) (4, 26).

The identified BXD2 autoepitope profile advances knowledge concerning the autoantibody repertoire in the BXD2 mice. Common lupus associated autoantigens such as snRNP, smD1, CENP-A, and Ro52 were represented by 53, 37, 39 and 46 reported B-cell linear epitopes on the microarray, respectively (Fig. 1*C*). This extensive coverage allowed identification of multiple BXD2 positive epitopes on a given autoantigen. Antigens displaying extensive reactivity with BXD2 serum (six or greater positive epitopes) were 70 kDa U1RNP, smD1, CENP-A, and Ro52 (Fig. 1*C*). Similarly, the inclusion of citrulline-modified variants in the

array content revealed that pooled BXD2 serum was reactive with a citrullinated and a non-citrullinated version of fibromodulin, fibrinogen-β and BiP peptides (Fig. 1*D*). This finding is consistent with reports that human autoantibodies recognize both an uncitrullinated and citrullinated variant of peptides deriving from common autoantigens (31, 32).

Strategies for selection of linear autoepitopes for further analysis

Given that the number of potential autoepitopes in BXD2 mice is extremely large, further analysis required development of an efficient, high throughput strategy that would generate the data required for informed selection of the linear autoepitopes of interest. A secondary microarray was printed that included linear peptides representing the predominant epitopes identified in the original screening of pooled BXD2 sera, encompassing peptides from the three major categories of proteins targeted by BXD2 autoantibodies and present in human disease (33), i.e., nuclear, matrix and enzyme/chaperone antigens (Table 1).

As class switching is associated with the production of pathogenic autoantibodies (34), the secondary microarrays were probed with serum from individual BXD2 mice and control normal B6 mice using an isotype-specific analysis (Fig. 2). In addition, because the emergence of class-switched, pathogenic autoantibodies follows a well-defined age-associated progression in BXD2 mice (4), sera from BXD2 mice of different ages and age-matched B6 controls were included in this assay. The results obtained from analysis of BXD2 sera indicated an increase in IgG autoantibodies to peptides deriving from nuclear autoantigens, with highest levels of anti-La, RNP and Ro60 in older BXD2 mice (Fig. 2*A*, 2*B*). The predominant nuclear peptides that were reactive with BXD2 sera were associated with a cluster of key antigens, including La, the U1snRNP complex, Ro60, CENP-A/E, DNA topoisomerase, and RNA polymerase II (Fig. 2*A*). Epitopes derived from matrix proteins fibrinogen-β and fibromodulin (Fig. 2*C*) and enzyme proteins BiP and clusterin (Fig. 2*D*) were positive in most BXD2 mice.

In contrast to the IgG autoantibodies, which were detected largely in BXD2 mice only, IgM autoantibodies were broadly present in both B6 and BXD2 mice (Fig. 2 Supplementary Fig. 1). These results are consistent with the previously described age-associated emergence of class-switched Ro60, followed by heat-shock proteins including BiP, and finally histone and DNA autoantibodies in BXD2 mice (4).

Verification of epitopes using synthesized peptides

To verify that the peptides discovered by screening the epitope microarray are authentic epitopes, selected peptides were synthesized with an N-terminal biotin (Table 2). These biotinylated peptides were analyzed for reactivity with IgM and IgG autoantibodies in the sera of B6 and BXD2 mice by standard ELISA and ELISPOT analyses. For these assays, we used high-binding capacity (HBC) neutravidin coated 96-well plates for anti-peptide antibody detection. Using this modified ELISA, we found significantly higher levels of IgG autoantibodies directed against all tested linear epitopes from BiP, histone, CENP-A, La, snRNP as well as structural antigen epitopes fibrinogen-β-cit and fibromodulin-cit in the sera of 7–9 month-old BXD2 compared to younger BXD2 mice and normal B6 mice (Fig. 3*A*, 3*B*). Also, consistent with the microarray data, we found IgM autoantibody reactivity

with all peptides tested and, for most peptides, a lack of elevation in the levels of these autoantibodies between young or old B6 mice compared to young or old BXD2 mice (Fig. 3*C*).

Using the modified ELISPOT, we also were able to enumerate anti-peptide antibody producing B cells from the spleens of 5–6 month old B6 and BXD2 mice, and observed a significantly increased number of IgG producing B cells from BXD2 mice that were reactive with $La_{13–27}$, histone $H1b_{205–219}$, and $snRNP_{357–373}$, which was increased by stimulation with PMA + ionomycin (Fig. 3*D*). There were, however, little to no detectable IgG producing autoantibody-reactive B cells from B6 mice (Fig. 3D). For IgM isotype ELISPOT analysis, under unstimulated condition, there was a significantly lower number of IgM spots for $H1b_{205–219}$ and $snRNP_{357–373}$ in BXD2 compared to B6 mice (Fig. 3*E*).

Construction of tetramers and strategy for gating analysis

From the above assays, the $La_{13–27}$ epitope was selected for construction of an autoepitope tetramer using a protocol modified from Taylor et al (21). Briefly, a 10–20 fold molar excess of biotinylated peptide was conjugated to R-phycoerythrin (PE)–labeled streptavidin (SA). To exclude cells binding irrelevant epitopes on PE or streptavidin, a non-specific tetramer was also produced by conjugating Alexa Fluor 647 (AF647) to SA-PE loaded with biotin to block free binding sites. For all tetramer experiments, single-cell suspensions were co-stained with the non-specific biotin-PE*AF647 tetramer and the peptide-PE tetramer to discriminate between peptide-binding and non-specific binding (21). Lymphocytes were gated by forward and side scatter, followed by exclusion of doublets, non-viable cells, and non-B cells. The resulting two-dimensional plot with biotin-PE*AF647 non-specific tetramer on the y-axis and the peptide PE-tetramer on the x-axis yields a small population of $La_{13–27}$ binding B cells (Fig. 4*A*). To test the specificity of tetramer-labeled B cells, cells were pre-incubated with free peptide prior to tetramer staining. Pre-incubation of cells with $La_{13–27}$ but not irrelevant $OVA_{323–339}$ peptide, resulted in a significant decrease in $La_{13–27}$ tetramer-stained cells (Fig. 4*B*, 4*C*).

Because epitope specific B cells are rare events within the B6 and BXD2 polyclonal repertoire (Fig. 4*D*, left panels), tetramer-stained cells were enriched with magnetic anti-PE beads and a magnetized MACS column using the protocol described by Taylor et al (21). While most cells obtained in the final enriched fraction bind nonspecifically to the column or Biotin-PE*AF647 tetramer, a smaller number of cells bind only the peptide-PE tetramer. This tetramer enrichment strategy enables isolation and analysis of rare peptide-specific B cells with significantly increased sensitivity as compared to a similar analysis of pre-enriched B cells and column flow-thru fractions (Fig. 4*D*, 4*E*). A similar method was used to generate, enrich and determine the B-cell binding specificity of a second $snRNP_{357–373}$ tetramer (Supplementary Fig. 2).

Increased $La_{13–27}$ and $snRNP_{357–373}$ reactive in selective B cell subsets in BXD2 mice

Identifying a BXD2 autoepitope repertoire for tetramer design enables study of epitope-reactive B cells in non-transgenic autoimmune mice. We therefore tested this approach in a proof-of-principle study designed to determine if autoantigen-reactive B cells are skewed

towards separate B-cell subsets in B6 and BXD2 mice. Based on results from the aforementioned analyses, epitopes derived from La and snRNP were selected. These two RNA binding protein autoantigens are targets of human SLE autoantigens (6) and are present in apoptotic debris (35, 36). Tetramer-reactive cell populations were gated as described in Figure 4. There were comparable percentages of $La_{13–27}$ or $snRNP_{357–373}$ reactive B cells in the spleen of 6-8-mo-old B6 and BXD2 mice (Fig. 5*A*), though the total numbers of $La_{13–27}{}^{+}$ or $snRNP_{357–373}{}^{+}$ B cells were significantly higher in the spleen of BXD2 mice (Fig. 5*B*) as a result of splenomegaly in these mice (37).

We have shown previously that $IgM^{hi}CD21^{hi}CD23^{hi}$ marginal zone precursor (MZ-P) B cells can capture and present Ags derived from mOVA apoptotic debris to directly stimulate OT-II TCR- specific CD4 T cells (38). We also have shown previously that splenic MZ-P B cells are increased in BXD2 mice and can capture and transport TNP antigen directly into the GC of BXD2 mice (39). As both MZ and MZ-P B cells are increasingly implicated in the pathogenesis of SLE (9, 40, 41) and both populations are critical in BXD2 autoreactive GC development (42), we analyzed expression of IgM, CD21, and CD23, markers (28) to delineate subsets of B cell that were reactive to $La_{13–27}$ and $snRNP_{357–373}$ peptides. From these analyses, both the $IgM^{hi}CD21^{hi}$ population, containing the MZ and MZ-P B subsets, as well as $IgM^{lo/–}CD21^{lo/–}$ population, containing the follicular (FO) B subset, were represented in the $tetramer^{+}$ population (Fig. 5*C*). There was an increased percent of $La_{13–27}$ and $snRNP_{357–373}$ reactive IgM^{int} and IgM^{lo} FO B cells in the BXD2 mouse compared to B6 mouse. Furthermore, within the $IgM^{hi}CD21^{hi}$ population that contains both $IgM^{hi}CD21^{hi}CD23^{lo/–}$ MZ and $IgM^{hi}CD21^{hi}CD23^{+}$ MZ-P, there was a significant increase in the percentage of $La_{13–27}$ and $snRNP_{357–373}$ tetramer-reactive $CD23^{hi}$ MZ-P B cells in BXD2 mice (Fig. 5*C*). There were also significantly increased numbers of $La_{13–27}{}^{+}$ and $snRNP_{357–373}{}^{+}$ MZ-P B cells in the BXD2 mouse spleen (Fig. 5*D*). These results are consistent with our previous finding that BXD2 mice have a higher frequency and greater number of FO and MZ-P B cells than B6 mice (42) and further demonstrate that a fraction of these cells exhibit reactivity to $La_{13–27}$ and $snRNP_{357–373}$ epitopes.

In vivo studies by other investigators have shown that counter selection against autoreactivity may take place at the transitional stage of B-cell development (43, 44). We further used CD93 (AA4) marker in combination with CD23 and sIgM staining to determine if there is abnormal deletion or selection of a transitional T1, T2 or T3 population of B cells within $tetramer^{+}$ B cells in BXD2 mice. The results show that while T1 is the dominant $La_{13–27}{}^{+}$ or $snRNP_{357–373}{}^{+}$ population of $CD93^{+}$ transitional B cells from B6 mouse spleens, there was abnormal skewing of $La_{13–27}{}^{+}$ and $snRNP_{357–373}{}^{+}$ B cells to the T3 population in BXD2 mice (Fig. 5*E*, 5*F*). Such abnormal expansion of T3 transitional B cells is also observed in the total B cell population in BXD2 mice (Supplementary Fig. 3*A*, 3*B*).

Increased activation and maturation of $La_{13–27}$ reactive B cells in BXD2 mice

The unusual expansion of MZ-P B cells and otherwise anergic T3 B cells (45) in BXD2 mice suggests that specific activation signals must exist to lead to expansion of these antigen-specific B cells. We showed previously that type I IFN-mediated upregulation of CD69 and down-regulation of S1P1 results in their inward migration from the MZ into the

follicle (40) where higher CD86 expression enables CD4 T-helper cell stimulation (46). We therefore analyzed if the $La_{13–27}$ -reactive and $snRNP_{357–373}$ -reactive MZ-P B cells exhibited an activation phenotype characterized by CD69 and CD86 expression. Compared to B6 mice, there was a significant upregulation of CD69 and CD86 in the tetramer$^+$ MZ-P B cell population in BXD2 mice (Fig. 6*A*, 6*B*). Similar analysis of these markers in the tetramer$^+$ IgM$^{lo/–}$CD21$^{lo/–}$ compartment, containing mainly FO and potentially GC B cells, revealed a slight increase in CD86, but not CD69 expression on both $La_{13–27}$ and $snRNP_{357–373}$ reactive cells (Fig. 6*A*, 6*B*). These results demonstrate that autoantigen $La_{13–27}$ and $snRNP_{357–373}$ specific MZ-P B cells in BXD2 mice exhibit upregulation of CD69 and CD86.

As ELISPOT analysis demonstrated significantly elevated numbers of IgG anti-$La_{13–27}$ and anti-$snRNP_{357–373}$ producing B cells, one important question is whether tetramer$^+$ B cells from BXD2 mice can mature into IgG secreting cells reactive with the peptide epitope and the whole self-Ag when under appropriate stimulation. This was tested by sorting of $La_{13–27}{}^+$ B cells, non-specific PE*AF647$^+$$La_{13–27}{}^{+/–}$, and double negative PE*AF647^{neg}$La_{13–27}{}^{neg}$ B cell subsets, followed by stimulation of these cells *in vitro* with LPS + IL-4. We first tested cell culture supernatant reactivity against the $La_{13–27}{}^+$ peptide and an irrelevant histone H1b peptide ($His_{205–219}$). ELISA results verified that $La_{13–27}{}^+$ B cells indeed produced significantly higher levels of IgG antibodies that reacted specifically with the $La_{13–27}{}^+$ peptide, and not an irrelevant $His_{205–219}$ peptide. In contrast, the non-specific PE*AF647$^+$$La_{13–27}{}^{+/–}$ B cells produced low levels of antibodies for both $His_{205–219}$ and $La_{13–27}$ (Fig. 6*C*). The selective production of full-length 47 kDa La/SSB reactive IgG antibodies by LPS + IL-4 stimulated $La_{13–27}{}^+$ B cells but not other subsets of B cells was also verified using a western immunoblotting analysis using whole recombinant La/SSB (Fig. 6*D*).

Finally, we applied the current tetramer approach to determine if, *in vivo*, BXD2 mice indeed exhibited elevated numbers of mature and mutated B cells. This was carried out by analyzing the presence of CD80$^+$PD-L2$^+$ memory B cells within the $La_{13–27}$ and $snRNP_{357–373}$ reactive populations. B cells upregulating these two molecules have been shown to be enriched in isotype-switched cells and in highly mutated cells, even when IgM bearing (47). Using this classification, $La_{13–27}$ and $snRNP_{357–373}$ tetramer reactive B cells in BXD2 mice displayed a significantly higher frequency of CD80$^+$PD-L2$^+$ B cells compared to the counterpart B cells from B6 mice (Fig. 6*E*, 6*F*). There was also an increased frequency of CD80$^+$PD-L2$^+$ B cells in tetramer$^+$ cells compared to non-tetramer gated total B cells from BXD2 mice (Fig. 6*E*, 6*F*). Together, these results indicate that this tetramer approach can be used to identify abnormal development of autoreactive B cells at various developmental stages.

Discussion

In this study, we demonstrate a step-wise approach to enable enrichment, isolation and characterization of autoantigen-reactive B cells in a mouse model that spontaneously develops autoantibody-mediated systemic autoimmune disease (4, 48). We demonstrate that an IEDB based peptide array of 2,733 autoimmune disease associated B-cell epitopes can

reveal linear epitopes on known autoantigens in BXD2 mice. Further, the age-related emergence of class-switched autoantibodies identified using the peptide arrays paralleled previous observations using standard whole Ag ELISA assays (4). Moreover, the serum reactivity of a panel of these identified autoepitopes was confirmed using ELISA and ELISPOT analysis of synthetic peptides. Peptide reactive tetramer B cells can also be stimulated to produce IgG antibodies that react with the full-length protein antigen. In the future, tetramer$^+$ B cells and Ig genes from these cells would need to be analyzed at the single cell level to enable cloning and expression of the autoantibody to better determine the specificity of the tetramer$^+$ B cells.

The peptides identified as BXD2 autoepitopes by the epitope array assay indicate which of these may be considered to be immunodominant. Potentially, this apparent immunodominance may simply reflect the array assay conditions. However, the reactivity pattern of BXD2 autoantibodies showed a preference towards nuclear and RNP autoantigens. Since initial observations of autoantigen clustering in apoptotic blebs (49), there has been growing awareness that chemical and structural modifications to autoantigens during cell death and neutrophil NETosis may provide B cells with access to normally concealed epitopes that may drive an aberrant adaptive immune response (50–52). Multiple studies have demonstrated that the majority of autoantigens targeted in systemic autoimmune diseases are substrates for granzymes, particularly granzyme B (53–55), and La itself is cleaved during apoptosis (56, 57). Similarly, the 70 kDa fragment of U1snRNP, another hallmark autoAg in patients with SLE, is specifically cleaved by the caspase-3 during apoptosis. This cleavage converts the molecule into a truncated 40-kDa fragment and a smaller 96-residue C-terminal fragment (36, 58), containing the snRNP$_{357–373}$ epitope identified here as a major BXD2 autoAg. Notably, this particular epitope is located in a structurally disordered region of the protein, a characteristic which may influence antigen capture, processing, presentation and immune dominance during cellular processes, including apoptosis (59). The peptide array identification of these autoepitopes is consistent with our previous observations of defective apoptotic body clearance and the ability of MZ-P B cells to directly capture antigen derived from uncleared apoptotic debris in BXD2 mice (38).

The present peptide array results also provide a clear picture of the transition from autoreactive IgM to IgG in BXD2 mice and confirm that this transition is absent for most linear autoepitopes in B6 mice, as we have described previously for full-length autoantigens (4). The autoreactive IgG in BXD2 mice are highly pathogenic and form immune complexes that deposit in the kidney and joints (4). It should be noted, however, that the current studies were focused on the identification of antigen-specific subsets of autoreactive B cells. It has not yet been confirmed that the peptide-specific IgG autoantibodies that we identified are capable of forming pathogenic immune complexes or eliciting tissue damage.

The IgM autoantibody pattern, which is often overlooked, also revealed some interesting features. Although both B6 and BXD2 produce broadly autoreactive IgM, the IgM repertoire in both mice does exhibit specificity in that only some autoAg, but not all, are recognized. Thus, in both strains, IgM appears to recognize a similar set of key autoAgs. These results are consistent with the observation that autoreactive and polyreactive autoantibodies are

present both healthy and autoimmune humans (44, 60, 61), an observation not limited to IgM but occurring commonly even within the IgG memory B-cell pool (62, 63). These results suggest that BCR ability to recognize and engage self-Ag does not necessarily cause disease. However, within a permissive environment, as in the BXD2 mouse, even small perturbations in B-cell development, selection, or phenotype may drive normally benign autoreactivity toward an auto-toxic response. They further support the concept that while normal individuals may manifest some degree of autoimmunity to a set of self-antigens, this is benign as long as the regulatory capacity is intact (64).

Consistent with the detection of IgM autoantibodies in both B6 and BXD2 mice, most of the autoAg tetramer$^+$ B cells that are obtained directly from the spleen of a mouse are IgM$^+$. The most likely reason for this is that there is a larger population of splenic B cells that express both surface and secretory IgM compared to a relatively small number of IgG B cells that express both surface and secretory IgG (65). However, in the spleens of BXD2 mice, there is a decreased percentage of IgM^{hi} B cells compared to B6 mice. This is the case both within the pan-B cell population (39), as well as within the autoAg-reactive tetramer$^+$ B cell population (Fig. 5*C*).

Although there was an increase in the number of La and snRNP tetramer$^+$ B cells in the spleen of BXD2 mice compared to B6 mice, the percentages were not significantly different. However, the phenotype of these self-reactive tetramer$^+$ B cells in normal and autoimmune mice is different, which could be directed by autoantigen stimulation, effects of Type I IFN, and developmental differences. We propose that these phenotypic changes reflect common factors and events that are generally present in autoimmune disease.

The most prevalent population of tetramer$^+$ B cells in both B6 and BXD2 mice are IgM^{int} follicular (FO) B cells. These results are consistent with the finding that autoreactive B cells persist in the mature repertoire even in normal mice (66). Interestingly, compared to B6 mice, not only is there is a higher percent of IgM^{int} tetramer$^+$ B cells, but there also is a distinct population of IgM^{lo} tetramer$^+$ B cells in the BXD2 mouse spleens. In B6 mice, IgM^{lo} FO B cells are recently shown to be polyreactive B cells enriched for nuclear-reactive specificities (67). The presence of IgM^{lo} tetramer$^+$ B cells in BXD2 mice is consistent with our previous findings that pathogenic autoantibodies produced from BXD2 mice exhibit polyreactivity (4) and further suggests that these B cells may have derived from IgM^{hi} B cells which have encountered chronic autoantigen stimulation.

While La$_{13–27}$ and snRNP$_{357–373}$ reactive IgM^{hi} B cells from B6 mice are primarily the CD21^{hi}CD23^{lo} MZ B cells, the majority of these B cells in BXD2 mice display the CD21^{hi}CD23^{hi} MZ-P B cell phenotype. Furthermore, these Ag$^+$ MZ-P B cells are skewed toward a hyper-reactive CD86$^+$CD69$^+$ phenotype in BXD2. In mice, B cells with regulatory function have been observed within the transitional, B1 and marginal zone compartments (68). We have previously shown that while the expression of *Il10* and *Tgfb* was significantly higher, the expression of *Il6* was significantly lower in MZ-P B cells of B6 mice, compared to MZ-P B cells BXD2 mice (38). Consistent with this, CD23$^+$CD21^{hi}CD1d^{hi} B cells have been reported as the key pathogenic B cells in other mouse models of autoimmunity (69, 70). In contrast, Evans *et al.* demonstrated that MZ-P B cells from spleens of healthy naïve

DBA/1 mice adoptively transferred into immunized DBA/1 mice significantly prevented and ameliorated disease (71). This and other reports (72) of MZ-P-like B cell regulatory functions suggest that, in the non-autoimmune state, these cells may indeed serve a regulatory role. Regulatory roles of human B cells are less understood, but transitional B cells with an IL-10-mediated regulatory function have similarly been reported to be defective in patients with SLE (40). Increased $CD80^+$ and $CD86^+$ B cells also coincide with the observation that naïve populations of B cells from SLE patients appear to be activated (73).

Analysis of the $CD93^+$ transitional population of $La_{13–27}{}^+$ or $snRNP_{357–373}{}^+$ B cells in BXD2 mice further revealed that there is an abnormal expansion of T3 transitional B cells, a phenotype that has not been identified in other autoimmune mouse models (45). T3 B cells generally are considered not strictly transitional but anergic B cells maintaining self-tolerance through rapid turnover *in vivo* (74, 75). Interestingly, self-Ag stimulation has been shown to promote regression of mature B cells into the T3 compartment (75, 76). Thus, expansion of these cells coupled with abnormal T-cell help (25, 77) may present a risk for B-cell tolerance loss to $La_{13–27}$ or $snRNP_{357–373}$ in BXD2 mice. Consistent with the possible B-cell tolerance defects that can occur before or at the MZ-P B cell stage in BXD2 mice, there is an approximate three-fold increase of $CD80^+CD273^+$ memory/activated phenotype B cells in BXD2 mice compared to B6 mice. In contrast, the percentage of B cells with the $CD80^+CD273^+$ phenotype in BXD2 mice is enriched approximately six-fold in the $La_{13–27}{}^+$ and 20-fold in the $snRNP_{357–373}{}^+$ population compared to the same population in B6 mice. These results suggest that specific Ag stimulation can lead to expansion of an Ag-specific memory B cell population in BXD2 mice. $CD80^+$ $PD\text{-}L2^+$ memory B cells have been shown to differentiate rapidly into antibody producing B cells upon re-challenge without the need to go through another GC response (78). The present results may thus help to identify mechanisms related to the high titers of IgG autoantibody production in BXD2 mice.

The present proof-of-principle study establishes that the approach described in this work should provide a platform for integrating autoantibody profiles with underlying B-cell defects. The ability to collect and compare comprehensive global autoantibody profiles coupled with the utility of the tetramer approach provides a feasible strategy to address other clinically relevant questions. For example, $tetramer^+$ B cells and Ig genes from these cells should be analyzed at the single cell level to identify the differences between benign versus pathogenic autoreactive Ig sequences. Such observations may be highly applicable for characterization of autoreactive B cells in human disease, as $tetramer^+$ B cells that exhibit abnormal phenotypes can be detected in well-defined B cell subsets in human PBMCs (79).

Supplementary Material

Refer to Web version on PubMed Central for supplementary material.

Acknowledgments

This work was supported by a grant from Arthritis Foundation (to J.L.), Rheumatology Research Foundation, the Department of Veterans Affairs Merit Review Grant 1I01BX000600-01, the National Institutes of Health Grants

1AI 071110, and P30 AR048311 (to J.D.M.), and 1RO1 AI083705 (to H-C.H.). Flow cytometry data acquisition was carried out at the University of Alabama at Birmingham Comprehensive Flow Cytometry Core (supported by NIH grants P30-AR-048311 and P30-AI-027767). We thank Dr. Fiona Hunter for critical review of this manuscript.

Abbreviations used in this paper

SLE	systemic lupus erythematosus
RA	rheumatoid arthritis
RBP	ribonucleic acid binding protein
snRNP	small nuclear ribonucleoprotein
MZ-P	marginal zone precursor
SA	streptavidin
RNP	ribonucleoprotein
GC	germinal center
FO	follicular

References

1. Li QZ, Xie C, Wu T, Mackay M, Aranow C, Putterman C, Mohan C. Identification of autoantibody clusters that best predict lupus disease activity using glomerular proteome arrays. J Clin Invest. 2005; 115:3428–3439. [PubMed: 16322790]
2. Ferucci ED, Majka DS, Parrish LA, Moroldo MB, Ryan M, Passo M, Thompson SD, Deane KD, Rewers M, Arend WP, Glass DN, Norris JM, Holers VM. Antibodies against cyclic citrullinated peptide are associated with HLA-DR4 in simplex and multiplex polyarticular-onset juvenile rheumatoid arthritis. Arthritis Rheum. 2005; 52:239–246. [PubMed: 15641089]
3. Cheng Q, Mumtaz IM, Khodadadi L, Radbruch A, Hoyer BF, Hiepe F. Autoantibodies from long-lived 'memory' plasma cells of NZB/W mice drive immune complex nephritis. Ann Rheum Dis. 2013; 72:2011–2017. [PubMed: 24114925]
4. Hsu HC, Zhou T, Kim H, Barnes S, Yang P, Wu Q, Zhou J, Freeman BA, Luo M, Mountz JD. Production of a novel class of polyreactive pathogenic autoantibodies in BXD2 mice causes glomerulonephritis and arthritis. Arthritis Rheum. 2006; 54:343–355. [PubMed: 16385526]
5. Burlingame RW, Boey ML, Starkebaum G, Rubin RL. The central role of chromatin in autoimmune responses to histones and DNA in systemic lupus erythematosus. J Clin Invest. 1994; 94:184–192. [PubMed: 8040259]
6. Arbuckle MR, McClain MT, Rubertone MV, Scofield RH, Dennis GJ, James JA, Harley JB. Development of autoantibodies before the clinical onset of systemic lupus erythematosus. N Engl J Med. 2003; 349:1526–1533. [PubMed: 14561795]
7. Sanz I. Rationale for B cell targeting in SLE. Semin Immunopathol. 2014; 36:365–375. [PubMed: 24763533]
8. Anolik J, Sanz I. B cells in human and murine systemic lupus erythematosus. Curr Opin Rheumatol. 2004; 16:505–512. [PubMed: 15314486]
9. Palanichamy A, Barnard J, Zheng B, Owen T, Quach T, Wei C, Looney RJ, Sanz I, Anolik JH. Novel human transitional B cell populations revealed by B cell depletion therapy. J Immunol. 2009; 182:5982–5993. [PubMed: 19414749]
10. Shlomchik MJ. Sites and stages of autoreactive B cell activation and regulation. Immunity. 2008; 28:18–28. [PubMed: 18199415]
11. Franz B, May KF Jr, Dranoff G, Wucherpfennig K. Ex vivo characterization and isolation of rare memory B cells with antigen tetramers. Blood. 2011; 118:348–357. [PubMed: 21551230]

12. Goodnow CC. Transgenic mice and analysis of B-cell tolerance. Annu Rev Immunol. 1992; 10:489–518. [PubMed: 1590994]
13. Doucett VP, Gerhard W, Owler K, Curry D, Brown L, Baumgarth N. Enumeration and characterization of virus-specific B cells by multicolor flow cytometry. J Immunol Methods. 2005; 303:40–52. [PubMed: 16045923]
14. Townsend SE, Goodnow CC, Cornall RJ. Single epitope multiple staining to detect ultralow frequency B cells. J Immunol Methods. 2001; 249:137–146. [PubMed: 11226471]
15. Newman J, Rice JS, Wang C, Harris SL, Diamond B. Identification of an antigen-specific B cell population. J Immunol Methods. 2003; 272:177–187. [PubMed: 12505722]
16. Jacobi AM, Zhang J, Mackay M, Aranow C, Diamond B. Phenotypic characterization of autoreactive B cells--checkpoints of B cell tolerance in patients with systemic lupus erythematosus. PLoS One. 2009; 4:e5776. [PubMed: 19488401]
17. van de Stadt LA, van Schouwenburg PA, Bryde S, Kruithof S, van Schaardenburg D, Hamann D, Wolbink G, Rispens T. Monoclonal anti-citrullinated protein antibodies selected on citrullinated fibrinogen have distinct targets with different cross-reactivity patterns. Rheumatology (Oxford). 2013; 52:631–635. [PubMed: 23264551]
18. Zachary AA, Kopchaliiska D, Montgomery RA, Leffell MS. HLA-specific B cells: I. A method for their detection, quantification, and isolation using HLA tetramers. Transplantation. 2007; 83:982–988. [PubMed: 17460571]
19. Morris L, Chen X, Alam M, Tomaras G, Zhang R, Marshall DJ, Chen B, Parks R, Foulger A, Jaeger F, Donathan M, Bilska M, Gray ES, Abdool Karim SS, Kepler TB, Whitesides J, Montefiori D, Moody MA, Liao HX, Haynes BF. Isolation of a human anti-HIV gp41 membrane proximal region neutralizing antibody by antigen-specific single B cell sorting. PLoS One. 2011; 6:e23532. [PubMed: 21980336]
20. Holl TM, Yang G, Kuraoka M, Verkoczy L, Alam SM, Moody MA, Haynes BF, Kelsoe G. Enhanced antibody responses to an HIV-1 membrane-proximal external region antigen in mice reconstituted with cultured lymphocytes. J Immunol. 2014; 192:3269–3279. [PubMed: 24591365]
21. Taylor JJ, Martinez RJ, Titcombe PJ, Barsness LO, Thomas SR, Zhang N, Katzman SD, Jenkins MK, Mueller DL. Deletion and anergy of polyclonal B cells specific for ubiquitous membrane-bound self-antigen. J Exp Med. 2012; 209:2065–2077. [PubMed: 23071255]
22. Robinson WH, DiGennaro C, Hueber W, Haab BB, Kamachi M, Dean EJ, Fournel S, Fong D, Genovese MC, de Vegvar HE, Skriner K, Hirschberg DL, Morris RI, Muller S, Pruijn GJ, van Venrooij WJ, Smolen JS, Brown PO, Steinman L, Utz PJ. Autoantigen microarrays for multiplex characterization of autoantibody responses. Nat Med. 2002; 8:295–301. [PubMed: 11875502]
23. Price JV, Haddon DJ, Kemmer D, Delepine G, Mandelbaum G, Jarrell JA, Gupta R, Balboni I, Chakravarty EF, Sokolove J, Shum AK, Anderson MS, Cheng MH, Robinson WH, Browne SK, Holland SM, Baechler EC, Utz PJ. Protein microarray analysis reveals BAFF-binding autoantibodies in systemic lupus erythematosus. J Clin Invest. 2013; 123:5135–5145. [PubMed: 24270423]
24. Cohen IR. Autoantibody repertoires, natural biomarkers, and system controllers. Trends Immunol. 2013; 34:620–625. [PubMed: 23768955]
25. Hsu HC, Yang P, Wang J, Wu Q, Myers R, Chen J, Yi J, Guentert T, Tousson A, Stanus AL, Le TV, Lorenz RG, Xu H, Kolls JK, Carter RH, Chaplin DD, Williams RW, Mountz JD. Interleukin 17-producing T helper cells and interleukin 17 orchestrate autoreactive germinal center development in autoimmune BXD2 mice. Nat Immunol. 2008; 9:166–175. [PubMed: 18157131]
26. Hsu HC, Yang P, Wu Q, Wang JH, Job G, Guentert T, Li J, Stockard CR, Le TV, Chaplin DD, Grizzle WE, Mountz JD. Inhibition of the catalytic function of activation-induced cytidine deaminase promotes apoptosis of germinal center B cells in BXD2 mice. Arthritis Rheum. 2011; 63:2038–2048. [PubMed: 21305519]
27. Kim Y, Ponomarenko J, Zhu Z, Tamang D, Wang P, Greenbaum J, Lundegaard C, Sette A, Lund O, Bourne PE, Nielsen M, Peters B. Immune epitope database analysis resource. Nucleic Acids Res. 2012; 40:W525–W530. [PubMed: 22610854]
28. Allman D, Pillai S. Peripheral B cell subsets. Curr Opin Immunol. 2008; 20:149–157. [PubMed: 18434123]

29. Winslow MM, Gallo EM, Neilson JR, Crabtree GR. The calcineurin phosphatase complex modulates immunogenic B cell responses. Immunity. 2006; 24:141–152. [PubMed: 16473827]
30. Vita R, Zarebski L, Greenbaum JA, Emami H, Hoof I, Salimi N, Damle R, Sette A, Peters B. The immune epitope database 2.0. Nucleic Acids Res. 2010; 38:D854–D862. [PubMed: 19906713]
31. Brink M, Hansson M, Ronnelid J, Klareskog L, Rantapaa Dahlqvist S. The autoantibody repertoire in periodontitis: a role in the induction of autoimmunity to citrullinated proteins in rheumatoid arthritis? Antibodies against uncitrullinated peptides seem to occur prior to the antibodies to the corresponding citrullinated peptides. Ann Rheum Dis. 2014; 73:e46. [PubMed: 24667899]
32. Shoda H, Fujio K, Shibuya M, Okamura T, Sumitomo S, Okamoto A, Sawada T, Yamamoto K. Detection of autoantibodies to citrullinated BiP in rheumatoid arthritis patients and pro-inflammatory role of citrullinated BiP in collagen-induced arthritis. Arthritis Res Ther. 2011; 13:R191. [PubMed: 22108001]
33. Plotz PH. The autoantibody repertoire: searching for order. Nat Rev Immunol. 2003; 3:73–78. [PubMed: 12511877]
34. Weinstein JS, Hernandez SG, Craft J. T cells that promote B-Cell maturation in systemic autoimmunity. Immunol Rev. 2012; 247:160–171. [PubMed: 22500839]
35. Reed JH, Jackson MW, Gordon TP. B cell apotopes of the 60-kDa Ro/SSA and La/SSB autoantigens. J Autoimmun. 2008; 31:263–267. [PubMed: 18511235]
36. Degen WG, Aarssen Y, Pruijn GJ, Utz PJ, van Venrooij WJ. The fate of U1 snRNP during anti-Fas induced apoptosis: specific cleavage of the U1 snRNA molecule. Cell Death Differ. 2000; 7:70–79. [PubMed: 10713722]
37. Mountz JD, Yang P, Wu Q, Zhou J, Tousson A, Fitzgerald A, Allen J, Wang X, Cartner S, Grizzle WE, Yi N, Lu L, Williams RW, Hsu HC. Genetic segregation of spontaneous erosive arthritis and generalized autoimmune disease in the BXD2 recombinant inbred strain of mice. Scand J Immunol. 2005; 61:128–138. [PubMed: 15683449]
38. Li H, Wu Q, Li J, Yang P, Zhu Z, Luo B, Hsu HC, Mountz JD. Cutting Edge: defective follicular exclusion of apoptotic antigens due to marginal zone macrophage defects in autoimmune BXD2 mice. J Immunol. 2013; 190:4465–4469. [PubMed: 23543760]
39. Wang JH, Li J, Wu Q, Yang P, Pawar RD, Xie S, Timares L, Raman C, Chaplin DD, Lu L, Mountz JD, Hsu HC. Marginal zone precursor B cells as cellular agents for type I IFN-promoted antigen transport in autoimmunity. J Immunol. 2010; 184:442–451. [PubMed: 19949066]
40. Blair PA, Norena LY, Flores-Borja F, Rawlings DJ, Isenberg DA, Ehrenstein MR, Mauri C. CD19(+)CD24(hi)CD38(hi) B cells exhibit regulatory capacity in healthy individuals but are functionally impaired in systemic Lupus Erythematosus patients. Immunity. 2010; 32:129–140. [PubMed: 20079667]
41. Landolt-Marticorena C, Wither R, Reich H, Herzenberg A, Scholey J, Gladman DD, Urowitz MB, Fortin PR, Wither J. Increased expression of B cell activation factor supports the abnormal expansion of transitional B cells in systemic lupus erythematosus. J Rheumatol. 2011; 38:642–651. [PubMed: 21239754]
42. J W. Marginal Zone Precursor B Cells as Cellular Agents for Type I IFN Promoted Antigen Transport in Autoimmunity. Journal of Immunology. 2010
43. Meffre E, Wardemann H. B-cell tolerance checkpoints in health and autoimmunity. Curr Opin Immunol. 2008; 20:632–638. [PubMed: 18848883]
44. Wardemann H, Yurasov S, Schaefer A, Young JW, Meffre E, Nussenzweig MC. Predominant autoantibody production by early human B cell precursors. Science. 2003; 301:1374–1377. [PubMed: 12920303]
45. Teague BN, Pan Y, Mudd PA, Nakken B, Zhang Q, Szodoray P, Kim-Howard X, Wilson PC, Farris AD. Cutting edge: Transitional T3 B cells do not give rise to mature B cells, have undergone selection, and are reduced in murine lupus. J Immunol. 2007; 178:7511–7515. [PubMed: 17548583]
46. Wang JH, Wu Q, Yang P, Li H, Li J, Mountz JD, Hsu HC. Type I interferon-dependent CD86(high) marginal zone precursor B cells are potent T cell costimulators in mice. Arthritis Rheum. 2011; 63:1054–1064. [PubMed: 21225691]

47. Tomayko MM, Steinel NC, Anderson SM, Shlomchik MJ. Cutting edge: Hierarchy of maturity of murine memory B cell subsets. J Immunol. 2010; 185:7146–7150. [PubMed: 21078902]
48. Hsu HC, Wu Y, Yang P, Wu Q, Job G, Chen J, Wang J, Accavitti-Loper MA, Grizzle WE, Carter RH, Mountz JD. Overexpression of activation-induced cytidine deaminase in B cells is associated with production of highly pathogenic autoantibodies. J Immunol. 2007; 178:5357–5365. [PubMed: 17404321]
49. Rosen A, Casciola-Rosen L, Ahearn J. Novel packages of viral and self-antigens are generated during apoptosis. J Exp Med. 1995; 181:1557–1561. [PubMed: 7699336]
50. Radic M, Marion T, Monestier M. Nucleosomes are exposed at the cell surface in apoptosis. J Immunol. 2004; 172:6692–6700. [PubMed: 15153485]
51. van Bavel CC, Dieker JW, Kroeze Y, Tamboer WP, Voll R, Muller S, Berden JH, van der Vlag J. Apoptosis-induced histone H3 methylation is targeted by autoantibodies in systemic lupus erythematosus. Ann Rheum Dis. 2011; 70:201–207. [PubMed: 20699234]
52. Khandpur R, Carmona-Rivera C, Vivekanandan-Giri A, Gizinski A, Yalavarthi S, Knight JS, Friday S, Li S, Patel RM, Subramanian V, Thompson P, Chen P, Fox DA, Pennathur S, Kaplan MJ. NETs are a source of citrullinated autoantigens and stimulate inflammatory responses in rheumatoid arthritis. Sci Transl Med. 2013; 5:178ra140.
53. Darrah E, Rosen A. Granzyme B cleavage of autoantigens in autoimmunity. Cell Death Differ. 2010; 17:624–632. [PubMed: 20075942]
54. Casciola-Rosen L, Andrade F, Ulanet D, Wong WB, Rosen A. Cleavage by granzyme B is strongly predictive of autoantigen status: implications for initiation of autoimmunity. J Exp Med. 1999; 190:815–826. [PubMed: 10499920]
55. Dudek NL, Maier S, Chen ZJ, Mudd PA, Mannering SI, Jackson DC, Zeng W, Keech CL, Hamlin K, Pan ZJ, Davis-Schwarz K, Workman-Azbill J, Bachmann M, McCluskey J, Farris AD. T cell epitopes of the La/SSB autoantigen in humanized transgenic mice expressing the HLA class II haplotype DRB1*0301/DQB1*0201. Arthritis Rheum. 2007; 56:3387–3398. [PubMed: 17907193]
56. Rutjes SA, Utz PJ, van der Heijden A, Broekhuis C, van Venrooij WJ, Pruijn GJ. The La (SS-B) autoantigen, a key protein in RNA biogenesis, is dephosphorylated and cleaved early during apoptosis. Cell Death Differ. 1999; 6:976–986. [PubMed: 10556975]
57. Huang M, Ida H, Kamachi M, Iwanaga N, Izumi Y, Tanaka F, Aratake K, Arima K, Tamai M, Hida A, Nakamura H, Origuchi T, Kawakami A, Ogawa N, Sugai S, Utz PJ, Eguchi K. Detection of apoptosis-specific autoantibodies directed against granzyme B-induced cleavage fragments of the SS-B (La) autoantigen in sera from patients with primary Sjogren's syndrome. Clin Exp Immunol. 2005; 142:148–154. [PubMed: 16178869]
58. Kattah NH, Kattah MG, Utz PJ. The U1-snRNP complex: structural properties relating to autoimmune pathogenesis in rheumatic diseases. Immunol Rev. 2010; 233:126–145. [PubMed: 20192997]
59. Pavlovic MD, Jandrlic DR, Mitic NS. Epitope distribution in ordered and disordered protein regions. Part B - Ordered regions and disordered binding sites are targets of T- and B-cell immunity. J Immunol Methods. 2014; 407:90–107. [PubMed: 24726865]
60. Shaw PX, Goodyear CS, Chang MK, Witztum JL, Silverman GJ. The autoreactivity of anti-phosphorylcholine antibodies for atherosclerosis-associated neo-antigens and apoptotic cells. J Immunol. 2003; 170:6151–6157. [PubMed: 12794145]
61. Silverman GJ. Regulatory natural autoantibodies to apoptotic cells: pallbearers and protectors. Arthritis Rheum. 2011; 63:597–602. [PubMed: 21360488]
62. Tiller. Autoreactivity in human IgG+ memory B cells. Immunity. 2007
63. Nagele EP, Han M, Acharya NK, DeMarshall C, Kosciuk MC, Nagele RG. Natural IgG autoantibodies are abundant and ubiquitous in human sera, and their number is influenced by age, gender, and disease. PLoS One. 2013; 8:e60726. [PubMed: 23589757]
64. Fattal I, Shental N, Mevorach D, Anaya JM, Livneh A, Langevitz P, Zandman-Goddard G, Pauzner R, Lerner M, Blank M, Hincapie ME, Gafter U, Naparstek Y, Shoenfeld Y, Domany E, Cohen IR. An antibody profile of systemic lupus erythematosus detected by antigen microarray. Immunology. 2010; 130:337–343. [PubMed: 20201986]

65. Morbach H, Eichhorn EM, Liese JG, Girschick HJ. Reference values for B cell subpopulations from infancy to adulthood. Clin Exp Immunol. 2010; 162:271–279. [PubMed: 20854328]

66. Zikherman J, Parameswaran R, Weiss A. Endogenous antigen tunes the responsiveness of naive B cells but not T cells. Nature. 2012; 489:160–164. [PubMed: 22902503]

67. Kirchenbaum GA, St Clair JB, Detanico T, Aviszus K, Wysocki LJ. Functionally responsive self-reactive B cells of low affinity express reduced levels of surface IgM. Eur J Immunol. 2014; 44:970–982. [PubMed: 24375379]

68. Fillatreau S, Gray D, Anderton SM. Not always the bad guys: B cells as regulators of autoimmune pathology. Nat Rev Immunol. 2008; 8:391–397. [PubMed: 18437156]

69. Moshkani S, Kuzin II, Adewale F, Jansson J, Sanz I, Schwarz EM, Bottaro A. CD23+ CD21(high) CD1d(high) B cells in inflamed lymph nodes are a locally differentiated population with increased antigen capture and activation potential. J Immunol. 2012; 188:5944–5953. [PubMed: 22593620]

70. Li J, Kuzin I, Moshkani S, Proulx ST, Xing L, Skrombolas D, Dunn R, Sanz I, Schwarz EM, Bottaro A. Expanded CD23(+)/CD21(hi) B cells in inflamed lymph nodes are associated with the onset of inflammatory-erosive arthritis in TNF-transgenic mice and are targets of anti-CD20 therapy. J Immunol. 2010; 184:6142–6150. [PubMed: 20435928]

71. Evans JG, Chavez-Rueda KA, Eddaoudi A, Meyer-Bahlburg A, Rawlings DJ, Ehrenstein MR, Mauri C. Novel suppressive function of transitional 2 B cells in experimental arthritis. J Immunol. 2007; 178:7868–7878. [PubMed: 17548625]

72. Yanaba K, Bouaziz JD, Haas KM, Poe JC, Fujimoto M, Tedder TF. A regulatory B cell subset with a unique CD1dhiCD5+ phenotype controls T cell-dependent inflammatory responses. Immunity. 2008; 28:639–650. [PubMed: 18482568]

73. Chang NH, McKenzie T, Bonventi G, Landolt-Marticorena C, Fortin PR, Gladman D, Urowitz M, Wither JE. Expanded population of activated antigen-engaged cells within the naive B cell compartment of patients with systemic lupus erythematosus. J Immunol. 2008; 180:1276–1284. [PubMed: 18178868]

74. Allman D, Lindsley RC, DeMuth W, Rudd K, Shinton SA, Hardy RR. Resolution of three nonproliferative immature splenic B cell subsets reveals multiple selection points during peripheral B cell maturation. J Immunol. 2001; 167:6834–6840. [PubMed: 11739500]

75. Merrell KT, Benschop RJ, Gauld SB, Aviszus K, Decote-Ricardo D, Wysocki LJ, Cambier JC. Identification of anergic B cells within a wild-type repertoire. Immunity. 2006; 25:953–962. [PubMed: 17174121]

76. Liubchenko GA, Appleberry HC, Holers VM, Banda NK, Willis VC, Lyubchenko T. Potentially autoreactive naturally occurring transitional T3 B lymphocytes exhibit a unique signaling profile. J Autoimmun. 2012; 38:293–303. [PubMed: 22365785]

77. Ding Y, Li J, Yang P, Luo B, Wu Q, Zajac AJ, Wildner O, Hsu HC, Mountz JD. Interleukin-21 promotes germinal center reaction by skewing the follicular regulatory T cell to follicular helper T cell balance in autoimmune BXD2 mice. Arthritis Rheumatol. 2014; 66:2601–2612. [PubMed: 24909430]

78. Zuccarino-Catania GV, Sadanand S, Weisel FJ, Tomayko MM, Meng H, Kleinstein SH, Good-Jacobson KL, Shlomchik MJ. CD80 and PD-L2 define functionally distinct memory B cell subsets that are independent of antibody isotype. Nat Immunol. 2014; 15:631–637. [PubMed: 24880458]

79. Kaminski DA, Wei C, Qian Y, Rosenberg AF, Sanz I. Advances in human B cell phenotypic profiling. Front Immunol. 2012; 3:302. [PubMed: 23087687]

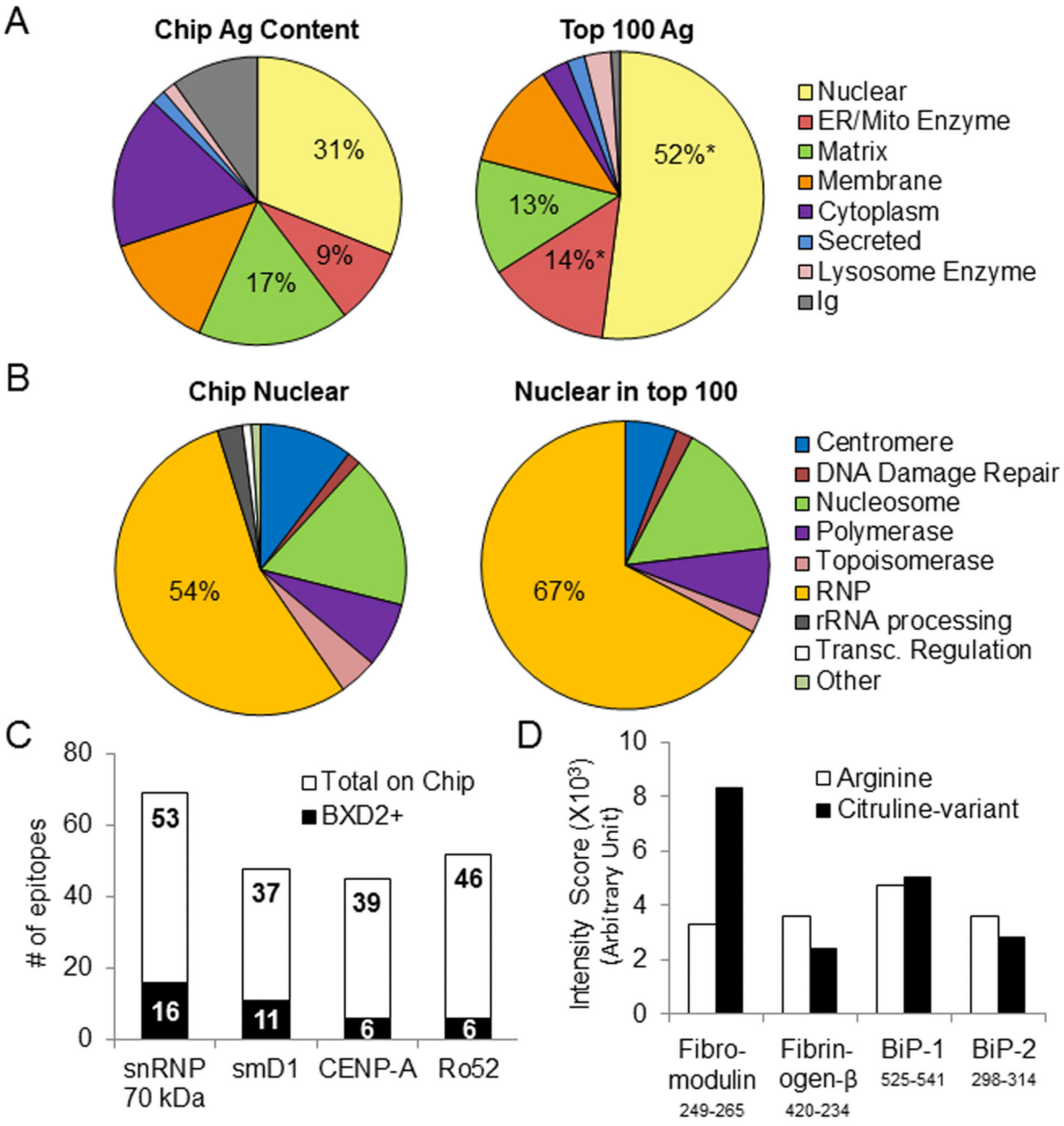

Fig. 1.

Autoantibody binding to peptide epitopes in BXD2 mice. An array containing 2,733 database derived linear peptide epitopes associated with autoimmune disease was probed with pooled sera (n=6). **A** Antigen content distribution of entire chip compared to top 100 BXD2 positive epitopes, where positive is defined as greater than five-fold above the mean intensity score. **B** Sub-classification of total chip nuclear antigens compared to top 100 BXD2 nuclear epitopes. **C** Number of BXD2 positive epitopes deriving from the indicated autoantigen. **D** BXD2 autoantibody binding intensity to un-citrullinated and citrulline

modified peptides deriving from the indicated autoantigen. * $P < 0.05$ between the antigen content distribution of the top 100 BXD2 epitopes vs. the distribution of the entire epitope microarray.

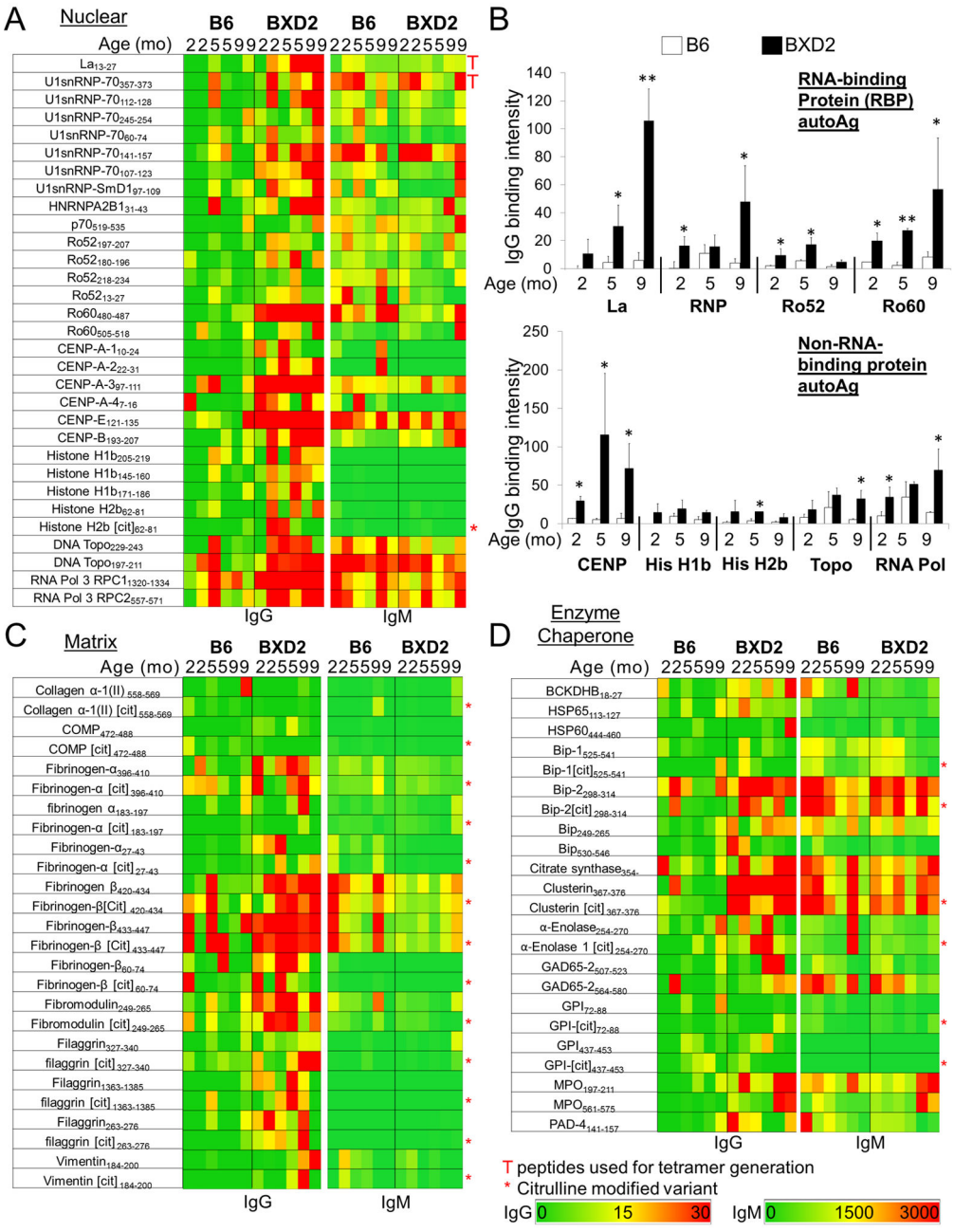

Fig. 2.

Autoreactive IgG and IgM signal intensities to peptide epitopes in BXD2 or control B6 mice at the indicated ages. Arrays were probed with serum (1:200 and 1:1000 for IgG and IgM analysis, respectively) from B6 or BXD2 mice at the indicated ages. **A** Heatmap of IgG and IgM signal intensities to peptides deriving from nuclear autoantigens. **B** B6 and BXD2 IgG signal intensities to epitopes from the indicated RNA-binding protein (RBP) autoantigen (top) and non-RBP nuclear Ag (bottom) at the indicated ages. Bars represent the average spot intensity (± SEM) of all epitopes deriving from the indicted autoantigen. * $P < 0.05$ and

** $P < 0.01$ between B6 and BXD2 of the same age. **C** Heatmap of IgG and IgM signal intensities to peptides deriving from matrix autoantigens. **D** Heatmap of IgG and IgM signal intensities to peptides deriving from enzyme or chaperone autoantigens.

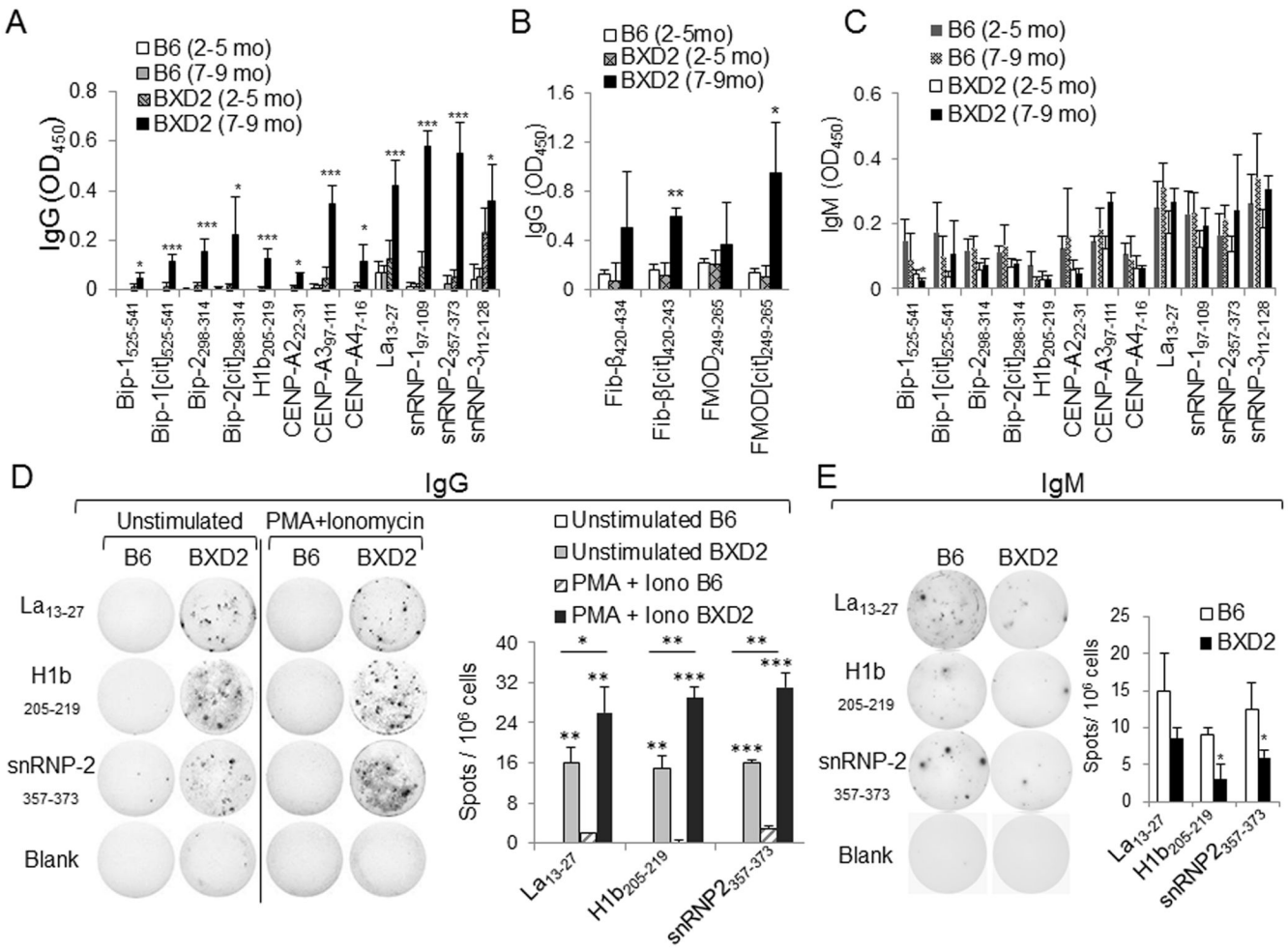

Fig. 3.

Verification of synthesized peptides. **(A-C)** ELISA of **A** IgG autoantibodies specific to BiP, histone, centromere, and ribonucleoprotein peptide epitopes; (**B**) IgG autoantibodies specific to fibrinogen and fibromodulin peptide epitopes, and **C** IgM autoantibodies specific to BiP, histone, centromere, and ribonucleoprotein peptide epitopes in the sera of B6 and BXD2 mice at the indicated ages. All data are the mean ± SEM of at least four mice per group. (**D, E**) ELISPOT assay of the **D** IgG or **E** IgM isotype autoantibody-producing B cells from B6 or BXD2 mice. Total spleen cells from 5–6 month-old B6 or BXD2 mice were cultured *in vitro* unstimulated (or stimulated with PMA + ionomycin in the IgG specific ELISPOT) on neutravidin ELISPOT plates coated with Lupus $La_{13–27}$, histone $H1b_{205–219}$ or $snRNP_{357–373}$. Right, mean ± SEM number of **D** IgG or **E** IgM autoantibody-forming spots. Results are data from 3–5 mice and at least two independent experiments. For all panels, * $P < 0.05$; ** $P < 0.01$; *** $P < 0.005$ versus control group (normal B6 mice or the indicated comparison).

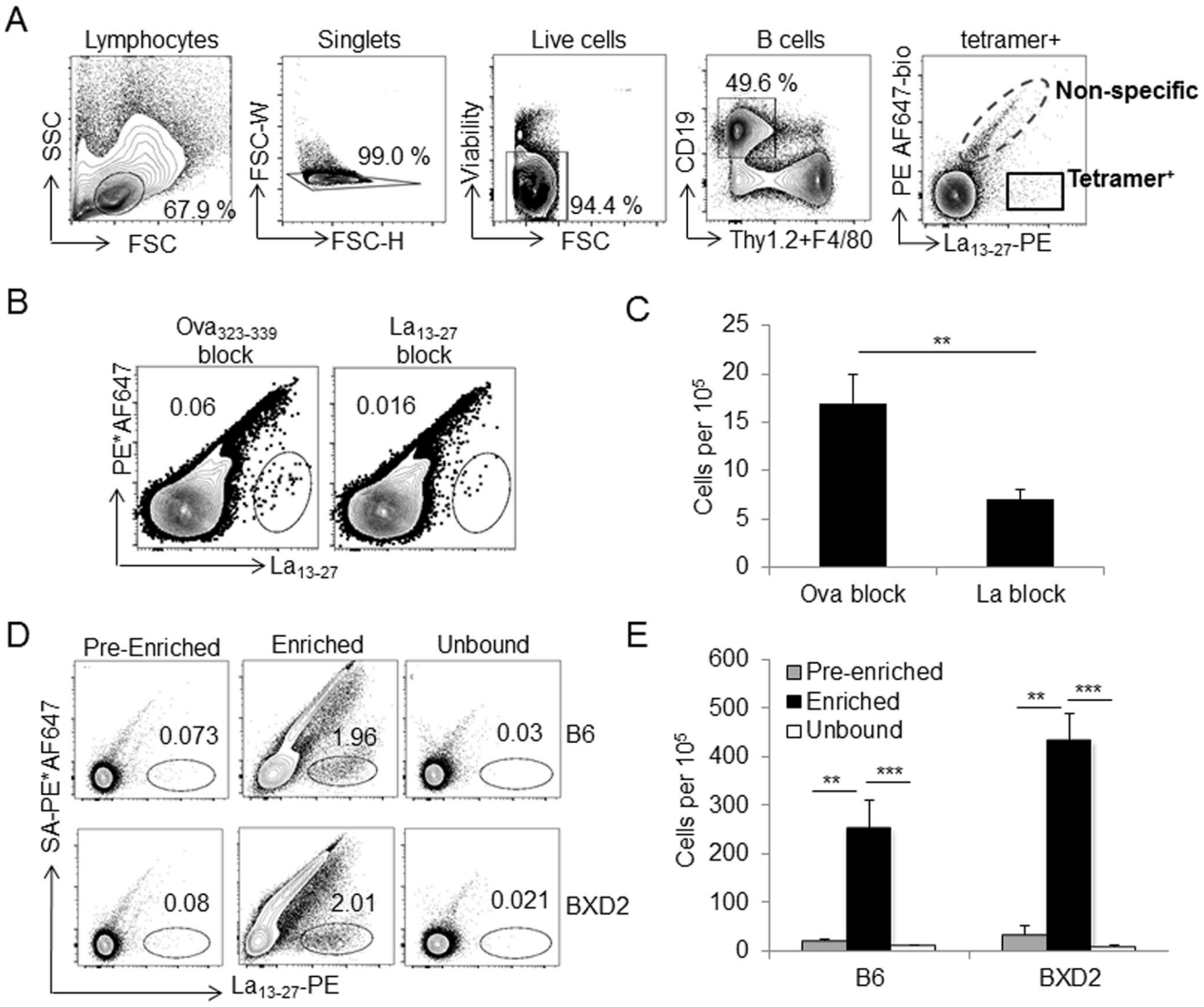

Fig. 4.

Tetramer enrichment and gating strategy. **A** Gating strategy for tetramer experiments. Cells were gated based on forward and side scatter (lymphocyte gate) and signal height and widths (doublet exclusion). B cells were selected as $CD19^+$ $F4/80^-$ $Thy1.2^-$. $Tetramer^+$ cells were identified as $PE*AF647^-$ and PE peptide-$tetramer^+$. The experiment and gating strategy shown are representative of similar tetramer experiments. **B, C** Cells were incubated with 300 μM of monomeric $La_{13–27}$ or 300 μM $OVA_{323–339}$ peptide 30 min before $La_{13–27}$ tetramer labeling. Representative tetramer gated plots analyzed by flow cytometry **B**, and bar graph showing the average of cell counts under each blocking condition (per 10^5 events analyzed) **C**. ** $P < 0.01$ compared to $OVA_{323–339}$ peptide blocked cells. **D, E** Enrichment of $tetramer^+$ B cells using anti-PE microbeads. Representative plots of enriched, pre-enriched, and flow-through fractions of $La_{13–27}^+$ cells **D**, and cell counts for plots shown in panel D (per 10^5 events analyzed) **E**. ** $P < 0.01$; ***

$P < 0.005$ compared to enriched or unbound fractions (N=3–5 from at least 2 independent experiments).

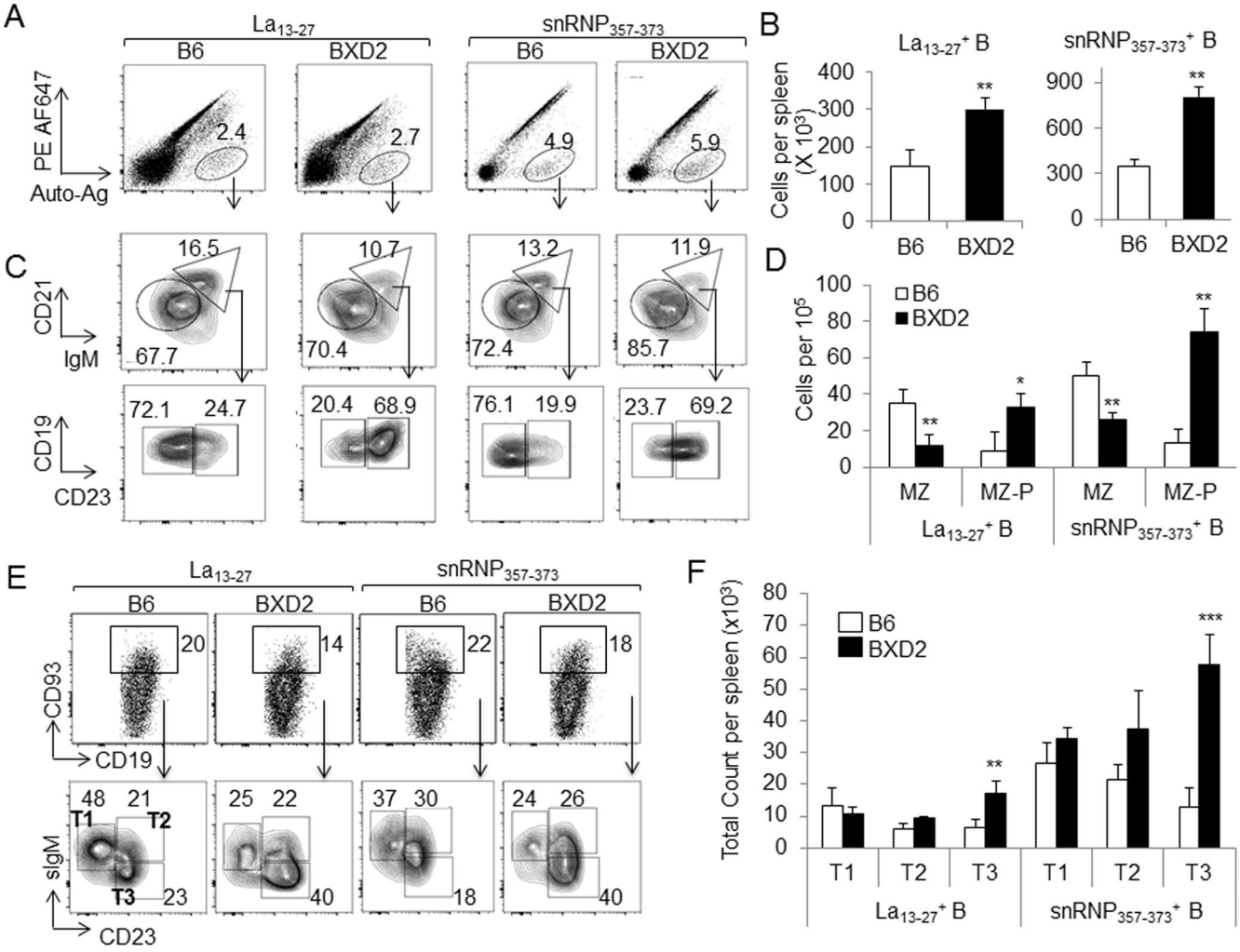

Fig. 5.

Increased $La_{13–27}$ and $snRNP_{357–373}$ tetramer$^+$ MZ-P and T3 B cells in BXD2 mice. **A** Spleen cells from 6–8 month old B6 and BXD2 mice were tetramer stained and enriched for FACS analysis of the frequency and number of $La_{13–27}$ or $snRNP_{357–373}$ tetramer$^+$ B cells. **B** Cell counts for $La_{13–27}$ and $snRNP_{357–373}$ tetramer$^+$ cells in total single cell suspension derived from the spleens of B6 and BXD2 mice. **C** $La_{13–27}$ and $snRNP_{357–373}$ tetramer$^+$ cells were further analyzed for the frequency of $IgM^{hi}CD21^{hi}$ B cells or $IgM^{lo/-}CD21^{lo/-}$ B cells (top panels). The $IgM^{hi}CD21^{hi}$ B cells were further gated into $IgM^{hi}CD21^{hi}$ $CD23^-$ MZ and $IgM^{hi}CD21^{hi}$ $CD23^+$ MZ-Ps (bottom panels), and the frequency of MZ or MZ-P B cells within this population is shown. **(D** Cell counts for $La_{13–27}$ and $snRNP_{357–373}$ tetramer$^+$ MZ and MZ-P cells in spleens of B6 and BXD2 mice (per 10^5 events analyzed). **E** FACS analysis showing the frequency of $La_{13–27}$ and $snRNP_{357–373}$ tetramer$^+$ transitional B cell subsets. **F** Cell counts for $La_{13–27}$ and $snRNP_{357–373}$ tetramer$^+$ T1, T2, and T3 B cells in spleens of B6 and BXD2 mice. Each panel is representative of 3–5 mice and at least two independent experiments. * $P < 0.05$ and ** $P < 0.01$ between B6 and BXD2.

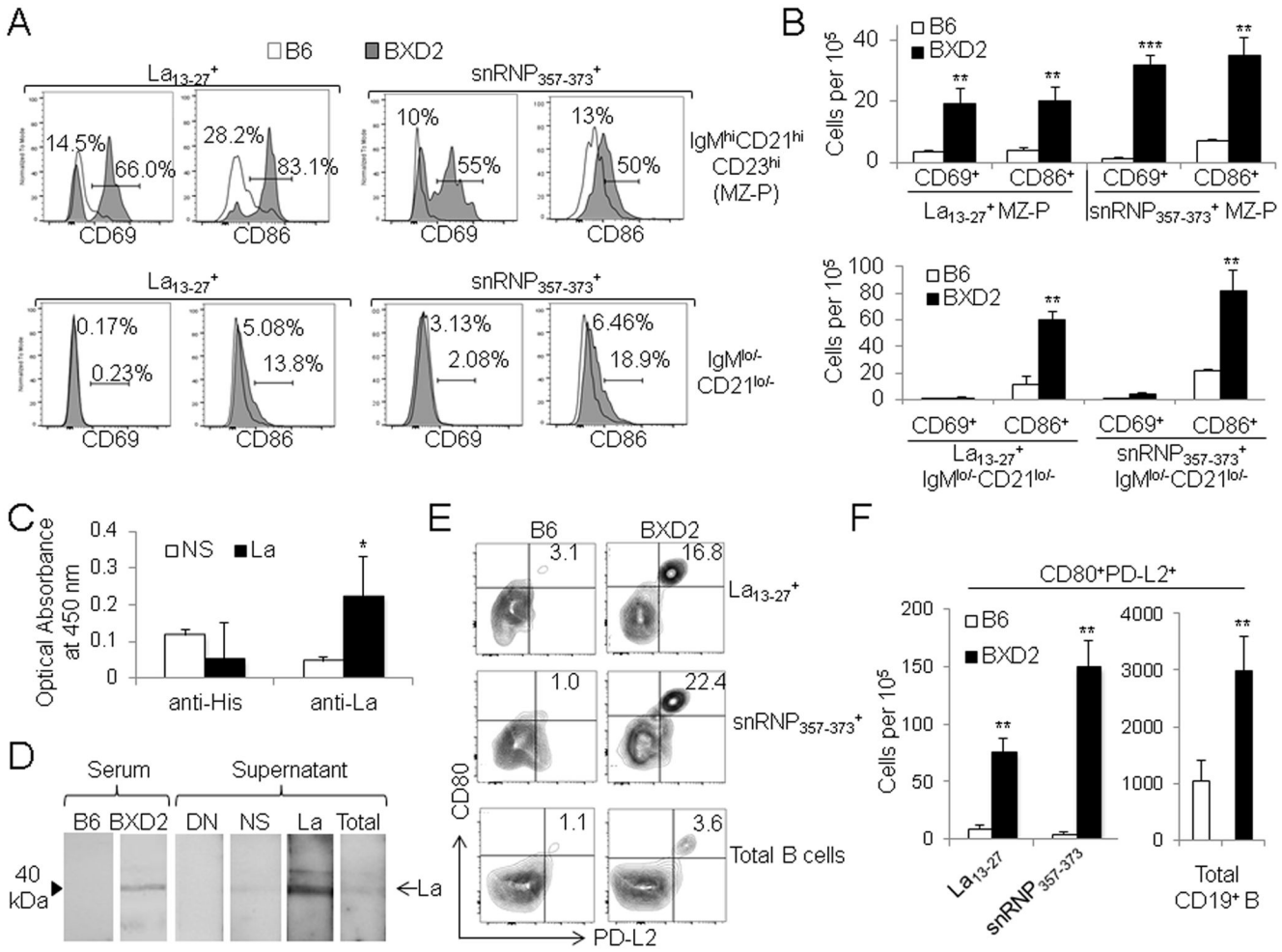

Fig. 6.

Increased percentage of activated tetramer$^+$ MZ-P and CD80$^+$PD-L2$^+$ memory B cells in BXD2 mouse spleens. **A)** Flow cytometry analysis of expression of CD69$^+$ and CD86$^+$ cells in $La_{13–27}{}^+$ and $snRNP_{357–373}{}^+$ MZ-P (top) and $IgM^{lo/–}CD21^{lo/–}$ (bottom) B cells from B6 and BXD2 mice. **B)** Cell counts for histograms in panel A (per 10^5 events analyzed). (**C**) ELISA analysis using supernatant collected from LPS + IL-4 stimulated sorted cell culture as the primary antibody to probe against Histone $H1b_{205–219}$ or $La_{13–27}$ peptide. NS = supernatant produced by non-specific tetramer$^+$ B cells; La = supernatant produced by $La_{13–27}{}^+$ B cells. **D** Western blotting analysis using B6 or BXD2 serum (1:50) or supernatant from LPS + IL-4 stimulated sorted cell culture as the primary antibody to probe against recombinant La antigen. DN = double tetramer negative supernatant; NS = non-specific tetramer$^+$ supernatant; La = $La_{13–27}{}^+$ supernatant. La protein loaded membranes were cut into individual strips to enable probing with supernatant from different populations of sorted cells. **(E** $La_{13–27}$ top) and $snRNP_{357–373}$ middle) tetramer$^+$ cells and total CD19$^+$ B cells (bottom) were analyzed for the frequency of CD80$^+$ PD-L2$^+$ memory B cells. **F** Mean cell counts for plots shown in E (per 10^5 events analyzed). Data are representative of 2–3

mice from at least two independent experiments. * $P < 0.05$; ** $P < 0.01$, and *** $P < 0.005$ between B6 and BXD2.

Table 1

List of autoantigen epitopes used for reactivity comparisons between B6 and BXD2 mice

Category A. Nuclear		
$Ag_{Residue}$	**Peptide**	**Uniprot ID**
$La_{13–27}$	LEAKICHQIEYYFGD*	P05455
U1snRNP-$70_{357–373}$	SHRSERERRRDRDRDRD*	P08621
U1snRNP-$70_{112–128}$	YDTTESKLRREFEVYGP*	P08621
U1snRNP-$70_{245–254}$	SRERDKERER	P08621
U1snRNP-$70_{60–74}$	AETREERMERKRRE	P08621
U1snRNP-$70_{141–157}$	GKPRGYAFIEYEHERDM	P08621
U1snRNP-$70_{107–123}$	VARVNYDTTESKLRREF	P08621
U1snRNP-SmD1$_{97–109}$	RGRGRGRGRGRGR	P62314
HNRNPA2B1$_{31–43}$	ETTEESLRNYYEQ	P22626
$p70_{519–535}$	GSLVDEFKELVYPPDYN	P12956
$Ro52_{197–207}$	LQELEKDEREQ	P19474
$Ro52_{180–196}$	AEFVQQKNFLVEEEQRQ	P19474
$Ro52_{218–234}$	LAQQSQALQELISELDR	P19474
$Ro52_{13–27}$	EVTCPICLDPFVEPV	P19474
$Ro60_{480–487}$	AIALREYR	P10155
$Ro60_{505–518}$	GFTIADPDDRGMLD	P10155
CENP-A-$1_{10–24}$	PEAPRRRSPSPTPTP	P49450
CENP-A-$2_{22–31}$	PTPGPSRRGP*	P49450
CENP-A-$3_{97–111}$	AAEAFLVHLFEDAYL*	P49450
CENP-A-$4_{7–16}$	SRKPEAPRRR*	P49450
CENP-$E_{121–135}$	PDREFLLRVSYMEIY	Q02224
CENP-$B_{193–207}$	SATETSLWYDFLPDQ	P07199
Histone H1b$_{205–219}$	KPKAAKPKKAAAKKK*	P10412
Histone H1b$_{145–160}$	ATPKKSAKKTPKKAKK	P10412
Histone H1b$_{171–186}$	KSPKKAKAAKPKKAPK	P10412
Histone $H2b_{62–81}$	IMNSFVTDIFERIASEASRL	P62807
Histone H2b $[cit]_{62–81}$	IMNSFVTDIFEZIASEASZL	P62807
DNA $Topo_{229–243}$	PPYEPLPENVKFYYD	P11387
DNA $Topo_{197–211}$	KEEEQKWKWWEEERY	P11387
RNA Pol 3 $RPC1_{1320–1334}$	SFEKTADHLFDAAYF	O14802
RNA Pol 3 $RPC2_{557–571}$	NTFRLMRRAGYINEF	Q9NW08

Category B. Matrix		
$Ag_{Residue}$	**Peptide**	**Uniprot ID**
Collagen α-1(II) 558–569	GARGLTGRPGDA	P02458

Category B. Matrix		
$Ag_{Residue}$	**Peptide**	**Uniprot ID**
Collagen α-1(II) $_{558–569}$	GARGLTGRPGDA	P02458
Collagen α-1(II) [cit] $_{558–569}$	GAZGLTGZPGDA	P02458
$COMP_{472–488}$	DDDNDGVPDSZDNCZLV	P49747
COMP [cit] $_{472–488}$	DDDNDGVPDSRDNCRLV	P49747
Fibrinogen-$α_{396–410}$	DSPGSGNARPNNPDW	P02671
Fibrinogen-α [cit] $_{396–410}$	DSPGSGNAZPNNPDW	P02671
fibrinogen $α_{183–197}$	SCSRALAREVDLKDY	P02671
Fibrinogen-α [cit] $_{183–197}$	SCSZALAZEVDLKDY	P02671
Fibrinogen-$α_{27–43}$	FLAEGGGVRGPRVVERH	P02671
Fibrinogen-α [cit] $_{27–43}$	FLAEGGGVZGPRVVERH	P02671
Fibrinogen $β_{420–434}$	PRKQCSKEDGGGWWY*	P02675
Fibrinogen-β[Cit] $_{420–434}$	PZKQCSKEDGGGWWY*	P02675
Fibrinogen-$β_{433–447}$	WYNRCHAANPNGRYY	P02675
Fibrinogen-β [Cit] $_{433–447}$	WYNZCHAANPNGZYY	P02675
Fibrinogen-$β_{60–74}$	RPAPPPISGGGYRAR	P02675
Fibrinogen-β [cit] $_{60–74}$	ZPAPPPISGGGYZAZ	P02675
$Fibromodulin_{249–265}$	LYMEHNNVYTVPDSYFR*	Q06828
Fibromodulin [cit] $_{249–265}$	LYMEHNNVYTVPDSYFZ*	Q06828
$Filaggrin_{327–340}$	EQSRDGSRHPRSHD	P20930
filaggrin [cit] $_{327–340}$	EQSRDGSZHPRSHD	P20930
$Filaggrin_{1363–1385}$	QSADSSRHSGSGH	P20930
filaggrin [cit] $_{1363–1385}$	QSADSSZHSGSGH	P20930
$Filaggrin_{263–276}$	TGTSTGGRQGSHHE	Q03838
filaggrin [cit] $_{263–276}$	TGTSTGGZQGSHHE	Q03838
$Vimentin_{184–200}$	RLREKLQEEMLQREEAE	P08670

Category C. Enzyme/Chaperone		
$Ag_{Residue}$	**Peptide**	**Uniprot ID**
$BCKDHB_{18–27}$	GAEGHWRRLP	P21953
$HSP65_{113–127}$	EGMRFDKGYISGYFV	E5FHX3
$HSP60_{444–460}$	LLRVIPALDSLTPANED	P10809
Bip-$1_{525–541}$	TITNDQNRLTPEEIERM*	P11021
Bip-$1[cit]_{525–541}$	TITNDQNZLTPEEIERM*	P11021
Bip-$2_{298–314}$	ALSSQHQARIEIESFYE*	P11021
Bip-2[cit] $_{298–314}$	ALSSQHQAZIEIESFYE*	P11021
$Bip_{249–265}$	GDTHLGGEDFDQRVMEH	P11021
$Bip_{530–546}$	QNRLTPEEIERMVNDAE	P11021
Citrate $synthase_{354–363}$	DPRYTCQREF	O75390

Category C. Enzyme/Chaperone		
$Ag_{Residue}$	**Peptide**	**Uniprot ID**
Clusterin$_{367–376}$	NWVSRLANLTQGEDQYY	P10909
Clusterin [cit] $_{367–376}$	NWVSZLANLTQGEDQYY	P10909
α-Enolase$_{254–270}$	SGKYDLDFKSPDDPSRY	P06733
α-Enolase 1 [cit] $_{254–270}$	SGKYDLDFKSPDDPSZY	P06733
GAD65-2$_{507–523}$	WYIPPSLRTLEDNEERM	Q05329
GAD65-2$_{564–580}$	PAATHQDIDFLIEEIER	Q05329
GPI$_{72–88}$	AKSRGVEAARERMFNGE	P06744
GPI-[cit]$_{72–88}$	AKSZGVEAAZEZMFNGE	P06744
GPI$_{437–453}$	MRGKSTEEARKELQAAG	P06744
GPI-[cit]$_{437–453}$	MZGKSTEEAZKELQAAG	P06744
MPO$_{197–211}$	RWLPAEYEDGFSLPY	P05164
MPO$_{561–575}$	NQIAVDEIRERLFEQ	P05164
PAD-4$_{141–157}$	WGPCGQGAILLVNCDRD	Q9UM07

* Grey highlight, used in ELISA, ELISPOT, and/or tetramer analysis

[cit] or Z = citrullinated arginine

Table 2

Summary of epitopes used for ELISA, ELISPOT, and tetramer analyses

Peptide (Residue)	Abbreviation	Sequence	Confirmed by
Nuclear or stress-response related proteins			
Bip-$1_{525–541}$	Bip-1	TITNDQNRLTPEEIERM	E
Bip-1[cit]$_{525–541}$	Bip-1-cit	TITNDQNZLTPEEIERM	E
Bip-$2_{298–314}$	Bip-2	ALSSQHQARIEIESFYE	E
Bip-2[cit]$_{298–314}$	Bip-2-cit	ALSSQHQAZIEIESFYE	E
Histone $H1b_{205–219}$	H1b	KPKAAKPKKAAAKKK	E, ES
CENP-$A2_{22–31}$	CENP-A2	PTPGPSRRGP	E
CENP-$A2_{97–111}$	CENP-A3	AAEAFLVHLFEDAYL	E
CENP-$A4_{7–16}$	CENP-A4	SRKPEAPRRR	E
$La_{13–27}$	La	LEAKICHQIEYYFGD	E, ES, T
U1 snRNP Sm-$D_{97–109}$	snRNP-1	RGRGRGRGRGRGR	E
70 kDa U1snRNP$_{357–373}$	snRNP-2	SHRSERERRRDRDRDRD	E, ES, T
70 kDa U1snRNP$_{112–128}$	snRNP-3	YDTTESKLRREFEVYGP	E
Structural proteins			
Fibrinogen $B_{420–434}$	Fib-β	PRKQCSKEDGGGWWY	E
Fibrinogen $B_{420–434}$-[cit]	Fib-β-cit	PZKQCSKEDGGGWWY	E
Fibromodulin$_{249–265}$	FMOD	LYMEHNNVYTVPDSYFR	E
Fibromodulin$_{249–265}$-[cit]	FMOD-cit	LYMEHNNVYTVPDSYFZ	E

E=ELISA, ES=ELISPOT, T= Tetramer, [cit] or Z=citrullinated arginine